Oncogene (2011) 1–11

www.nature.com/onc

ORIGINAL ARTICLE

A novel tumor-derived SGOL1 variant causes abnormal mitosis and unstable chromatid cohesion

T Kahyo[1], M Iwaizumi[1,2], K Shinmura[1], S Matsuura[1,3], T Nakamura[4], Y Watanabe[5], H Yamada[1] and H Sugimura[1]

[1]First Department of Pathology, Hamamatsu University School of Medicine, Hamamatsu, Japan; [2]First Department of Medicine, Hamamatsu University School of Medicine, Hamamatsu, Japan; [3]Second Department of Medicine, Hamamatsu University School of Medicine, Hamamatsu, Japan; [4]Second Department of Surgery, Hamamatsu University School of Medicine, Hamamatsu, Japan and [5]Laboratory of Chromosome Dynamics, Institute of Molecular and Cellular Biosciences, University of Tokyo, Tokyo, Japan

Mitosis is the most conspicuous cell cycle phase, because it is the phase in which the dynamic physical distributions of cellular components into the two daughter cells occur. The separation of sister chromatids is especially important during mitosis, because of the extreme accuracy required for distribution to the next generation of cells. Shugoshin-like 1 (SGOL1) is a key protein in protecting sister chromatids from precocious separation. We have reported finding that chromosome instability is more likely in SGOL1-downregulated colorectal cancers, but it is still unknown whether there is an association between cancer and SGOL1 transcript variation. Here, we identified a novel SGOL1 variant, SGOL1-P1, in human colon cancer. The SGOL1-P1 transcript contains an exon-skip of exon 3 that results in a stop codon occurring within exon 4. Overexpression of SGOL1-P1 in HCT116 cells resulted in an increased number of cells with aberrant chromosome alignment, precociously separated chromatids and delayed mitotic progression, occasionally followed by inaccurate distribution of the chromosomes. These phenotypes, observed when SGOL1-P1 was present, were also observed very frequently in SGOL1-knockdown cells. Furthermore, the overexpression of SGOL1-P1 inhibited the localization of endogenous SGOL1 and cohesin subunit RAD21/SCC1 to the centromere. These results suggest that SGOL1-P1 may function as a negative factor to native SGOL1, and that abundant expression of SGOL1-P1 may be responsible for chromosomal instability.
Oncogene advance online publication, 2 May 2011; doi:10.1038/onc.2011.152

Keywords: chromosomal instability; colon cancer; mitosis; shugoshin; splicing variant

Introduction

Accurate separation of sister chromatids to opposite poles during mitosis is necessary to ensure euploidy in the daughter cells, because once the sister chromosomes have incorrectly separated, they cannot revert to their original distribution in the normal nucleus. Aberrant distribution of chromosomes into daughter cells induces chromosomal instability (CIN) and often leads to aneuploidy (Rajagopalan and Lengauer, 2004). CIN frequently occurs in human malignant tumors (Lengauer *et al.*, 1998) and it is a major cause of genomic instability in colorectal cancer (Grady, 2004). Two causes of CIN have been reported: a defect in the spindle assembly checkpoint (SAC) and a defect in centrosome replication, both of which can be induced by a mutation in a checkpoint gene or by an exogenous agent (Pihan and Doxsey, 1999; Shinmura *et al.*, 2008). As chromosomes are exposed to the greatest risk of CIN during mitosis, analysis of mitotic progression has become a focus of attention in the field of cancer research (Bharadwaj and Yu, 2004).

The function of the cohesin complex is to physically bind sister chromatids from the genomic replication phase of the cell cycle until segregation at anaphase (Nasmyth *et al.*, 2000). Although the bulk of cohesin is removed during prophase and prometaphase, centromere cohesin persists throughout metaphase (Waizenegger *et al.*, 2000) and is finally cleaved by separase during anaphase (Hauf *et al.*, 2001). Kinetochore fiber microtubules from bipolar spindle poles attach to sister chromatids at the kinetochore. When spindle microtubules fail to attach to the kinetochore, SAC instead functions to prevent premature chromatid segregation. The premature segregation is prevented by the recruitment of SAC proteins to unattached kinetochores, which inhibits the cleavage of cohesin complex through the signaling cascade (Peters, 2002).

Originally, shugoshin/MEI-S332 (Sgo1) was identified in *Drosophila* as a mutant, defective in sister chromatid cohesion in meiosis (Goldstein, 1980) and reported to enrich at the centromere until sister chromatids separate (Kerrebrock *et al.*, 1995; Moore *et al.*, 1998). Further studies revealed that Sgo1 is a protector of

Correspondence: Dr H Sugimura, First Department of Pathology, Hamamatsu University School of Medicine, 1-20-1 Handayama, Higashi-ku, Hamamatsu, Shizuoka 431-3192, Japan.
E-mail: hsugimur@hama-med.ac.jp
Received 3 October 2010; revised and accepted 26 March 2011

Rec8, a component of meiotic cohesin, in yeast (Kitajima *et al*., 2004; Marston *et al*., 2004; Rabitsch *et al*., 2004; Clift *et al*., 2009) and that it is essential for accurate sister chromatid separation during mitosis in vertebrates (Salic *et al*., 2004; Tang *et al*., 2004; Kitajima *et al*., 2005; McGuinness *et al*., 2005). Shugoshin-like (SGOL1) protein, the mammalian homolog of shugoshin, interacts with protein phosphatase 2A (PP2A), localizes in the centromeric region and prevents cohesin complex from precocious cleavage at the centromere through dephosphorylation of SA2, one of the cohesin subunits (Kitajima *et al*., 2006; Riedel *et al*., 2006). In a study on human cancer, we found that SGOL1 expression was decreased in colorectal cancer and that SGOL1-knockdown led to CIN in a colon cancer cell line (Iwaizumi *et al*., 2009). Furthermore, a crucial link between histone H2A phosphorylation and CIN through shugoshin has recently been discovered (Kawashima *et al*., 2010). These reports on shugoshin and SGOL1 indicate that shugoshin is a cross-species guardian at the centromere.

Many tumor-specific splicing products have been studied in a variety of tumors. Although a variant-generating model in cancer has been suggested (Mayr and Bartel, 2009), no common theory applicable in all cancers has ever been proposed. In addition to the major splicing variants A1 and A2, 527 and 561 amino acids, respectively, some short variants of SGOL1 have been analyzed, and it has been suggested that the short variants have a negative effect on the cohesion between sister chromatids (Suzuki *et al*., 2006). However, no association between disease and *SGOL1* transcript variants has ever been shown.

In this paper, we report a novel *SGOL1* variant that was detected preferentially in tumor tissue. Forced expression of the tumor-associated variant resulted in abnormal mitotic progression and premature separation between sister chromatids in a colon cancer cell line, as same as in SGOL1-knockdown cells, suggesting that the tumor-associated variant interferes with native SGOL1 and can serve as a target for treatment.

Results

SGOL1-P1 expressed in colon cancer

A variety of *SGOL1* variants have been registered in the NCBI protein database (Figure 1a). To investigate whether there is an association between colon cancer and a particular *SGOL1* transcript variant, a reverse transcription-polymerase chain reaction (RT–PCR) was performed with total RNA from specimens of human colon cancer (Figure 1b). Many types of amplified products were detected from tumor tissue, but only one or two variants were amplified from normal tissue, and several products were cloned and sequenced from tumor tissue. A novel *SGOL1* variant named *SGOL1-P1* was identified among the sequenced clones derived from the tumor tissue. The sequence data of *SGOL1-P1* have been submitted to the DDBJ (DNA Data Bank of Japan) database under accession numbers AB567656 and AB567657. The *SGOL1-P1* transcript lacks the exon 3 region and has a frameshift that causes a premature stop codon to occur within exon 4 (Supplementary Figure S1). PCR analysis using the primer specific for *SGOL1-P1* showed that the prevalence of *SGOL1-P1* expression was 6/46 (13.0%) in colon tumors and that no *SGOL1-P1* was expressed in the adjacent non-tumor tissue (Figure 1c). Total expression of other variants, except P1, was lower in the tumor tissue expressing *SGOL1-P1* than in paired non-tumor tissues (Figure 1d), indicating that the emergence of *SGOL1-P1* was not caused by acceleration of *SGOL1* gene expression. In addition, we isolated 1.75-fold more SGOL1-P1 clones, by a series of procedures including RT–PCR, TA-cloning, and picking and counting the colonies, than the SGOL1-A variants clones from tumors. This result excludes the possibility that the P1 is a rare and artificial transcript in human tumors; instead, it suggests that P1 variant affects the wild type SGOL1 as a dominant negative form in the clinical setting. SGOL1-P1 is composed of 59 amino acids, including the short coiled-coil region determined by the *Coils2* program (Lupas *et al*., 1991) (Figure 1e). This region is well conserved among vertebrates (Supplementary Figure S2). Interestingly, the *SGOL1-P1*-positive tumors were smaller than the *SGOL1-P1*-negative tumors (Figure 1f). None of the *SGOL1-P1*-positive tumors was larger than the average of the tumors as a whole. These results show that *SGOL1-P1* is preferentially expressed in colon cancer and that there is a correlation between *SGOL1-P1* expression and tumor size.

Aberrant chromosome alignment during mitosis in cells expressing SGOL1-P1

To investigate the effect of SGOL1-P1 on cell division, we overexpressed SGOL1-P1 in HCT116 cells, human colorectal cancer cells, and observed the mitotic cells. Interestingly, the chromosome mass in the SGOL1-P1-transfected cells appeared spread out and not to be precisely aligned with the metaphase plate (Figure 2a). According to previous papers, aberrant chromosome alignment was observed in SGOL1-knockdown cells (Salic *et al*., 2004; Tang *et al*., 2004; Kitajima *et al*., 2005, 2006). We therefore analyzed chromosome alignment at prometaphase and metaphase in detail in the present study in order to investigate the function of SGOL1-P1. For this analysis, chromosome alignment index was calculated on the basis of the shape of chromosomal mass (Figures 2a and b). The results of the morphometric analysis of the images acquired in the present study showed that the frequency distributions of the chromosome alignment index values of SGOL1-knockdown cells (SGOL1 RNAi) and SGOL1-P1-overexpressing cells were lower than those of the control cells (control RNAi) and the cells transfected with empty vector, respectively (Figures 2c–f). These results indicate that SGOL1-P1 overexpression leads to aberrant chromosome alignment, the same way as SGOL1-knockdown does. When the chromosomal mass is not positioned parallel to the horizontal plane, the

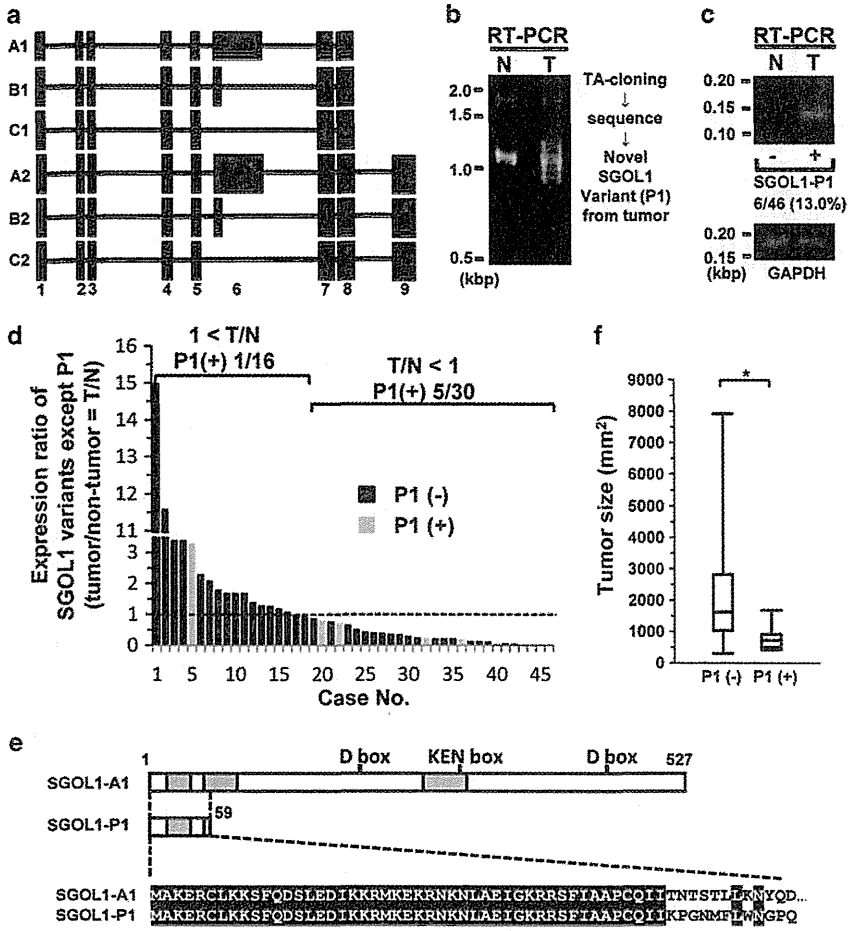

Figure 1 A novel SGOL1 variant expressed in colon cancer. (**a**) Scheme of SGOL1 transcript variants. Filled boxes represent exon regions (exons 1–9). (**b**, **c**) Total RNAs from colon cancer specimens were used to perform RT–PCR. Some products were amplified with the primers targeting exon 1 and exon 8 (**b**). Primers targeting the exon 2–4 junction and exon 5 of SGOL1 were also used (**c**). GAPDH was amplified as an internal control. N = non-tumor, T = tumor. (**d**) Quantitative real-time RT–PCR analysis of *SGOL1* variants, except P1. The primers targeting exon 3 and exon 4 of *SGOL1* were used. They are applicable for amplification of exon 3-containing *SGOL1* transcripts. (**e**) Amino acid alignment of SGOL1-A1 and SGOL1-P1. The gray areas indicate the coiled-coil regions. Both of D box and KEN box are known as motifs for destruction. The white letters on the black background represent amino acids that are identical in both variants. (**f**) Correlation between the presence of *SGOL1-P1* transcripts and tumor size. Tumor size was calculated by multiplying the length of the major axis by the length of the minor axis. P1(−), $n=40$; P1(+), $n=6$. $^*P<0.05$ (Mann–Whitney *U*-test).

calculated index value may not be appropriate for estimating the deviation of the chromosomes from the metaphasic plate. However, the distributions of the angles of the spindle bodies relative to the horizontal plane were similar among the various groups of cells that were examined (Supplementary Figure S3). Thus, the angle of the chromosomal mass relative to the horizontal plane may not have influenced the calculated index values in the present study.

Delayed mitotic progression in cells expressing SGOL1-P1

As the aberrant alignment in Figure 2a resembled the mitotic progression defect observed in SGOL1-knockdown cells reported previously (Salic *et al.*, 2004; McGuinness *et al.*, 2005), we performed time-lapse imaging to investigate the aberrant chromosome alignment, and we used GFP-histone H2B to observe the chromosome dynamics in living cells (Kanda *et al.*, 1998). Measurements of the time taken to progress from prophase to anaphase revealed severe mitotic arrest in SGOL1-knockdown cells (Figure 3a). It took 50 min or more for 50% of the cells (52/105) to move from prophase to anaphase. Most of the cells exhibiting this delayed phenotype (34/52, 65.4%) had not reached anaphase within the observation period, because prometaphase or metaphase had lasted several hours or more. The cells transfected with SGOL1-P1 also showed a progression delay compared with the cells transfected with SGOL1-A1 and the cells transfected with the empty control vector (Figure 3b). The subfraction of cells whose progression time between prophase and anaphase was 50 min or more was larger among the cells

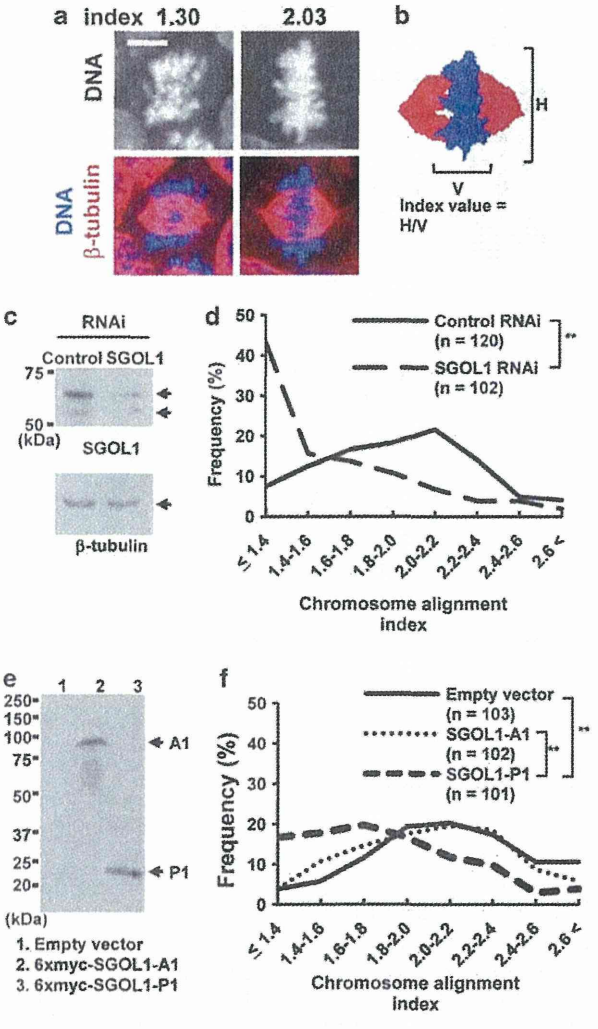

Figure 2 Aberrant chromosome alignment in mitotic cells expressing SGOL1-P1. (**a**) HCT116 cells were transfected with pSilencer-SGOL1 and myc-SGOL1 (A1 and P1) for knockdown and overexpression, respectively. Following antibiotic selection, the cells were subjected to immunofluorescence staining with anti-β-tubulin antibody and DAPI, and Z-stacked confocal images were acquired. Representative fluorescence images of the mitotic cells transfected with myc-SGOL1-P1 (left) and myc-SGOL1-A1 (right) are shown. Scale bar = 5 μm. (**b**) The chromosome alignment index was calculated as H/V, in which H and V are the horizontal length and vertical length, respectively, of the chromosomal mass at the metaphase plate. The blue area and the red areas represent the chromosomal mass and the spindle body, respectively. (**c**, **e**) Immunoblotting with rabbit anti-shugoshin antibody (**c**) and anti-myc antibody (**e**) was performed to confirm the effect of transfection. The graphs indicate frequency distribution of the ranges of chromosome alignment index values (**d**, **f**). $^{**}P<0.01$ (χ^2-test).

transfected with SGOL1-P1 (8/102, 7.84%) than among the cells transfected with SGOL1-A1 (3/125, 2.40%) or the cells transfected with the empty control vector (2/116, 1.72%). The chromosomes of the cells that exhibited delayed progression seemed to fumble for the metaphase plate (Figures 3c and d, and Supplementary Movie 1). The chromosomal masses in some SGOL1-P1 transfected cells (3/102, 2.94%) separated without congressing at the metaphase plate, but no such cells were observed among the cells transfected with SGOL1-A1 or the empty control vector (Figure 3e and Supplementary Movie 2). These results show that SGOL1-P1 expression prevents mitotic progression to anaphase and causes inaccurate chromosome distribution.

Decrease in centromeric localization of endogenous SGOL1 in cells expressing SGOL1-P1

Overexpressed SGOL1-P1 was localized in both the cytoplasm and the nucleus at interphase and outside the chromosomes during mitosis (Figure 4a). Furthermore, SGOL1-P1 was abundantly present even at anaphase (Figure 4a and Supplementary Figure S4a), whereas endogenous SGOL1 was not observed as described previously (Salic *et al.*, 2004). SGOL1-P1 lacks the motifs for destruction that are present in the long form of SGOL1 (Figure 1e; Karamysheva *et al.*, 2009). Therefore, the result that SGOL1-P1 was abundantly present at anaphase is consistent with its amino acid sequence. In some cases, abnormal segregations of chromosomes, such as that shown in Figure 3e, were observed in the SGOL1-P1-expressing cells (Figure 4a). The cyclin B1 level in cells exhibiting abnormal chromosome segregation was higher than that in cells exhibiting typical anaphase and similar to the level observed in metaphase cells (Supplementary Figure S4b). The anaphase-promoting complex/cyclosome (APC/C), which is a ubiquitin-ligase and targets cell-cycle-related proteins (including cyclin B1) for degradation by the 26S proteasome and promotes exit from metaphase, is suppressed during SAC activation (Wasch *et al.*, 2010). Therefore, our results show that abnormal chromosome segregation did not follow the degradation of cyclin B1, suggesting that SAC remains activated in cells in which abnormal chromosome segregation occurs. To investigate the effect of SGOL1-P1 on endogenous SGOL1 at mitosis, we performed a co-immunofluorescence study for the centromere, endogenous SGOL1 and myc-SGOL1-P1. Interestingly, we found that the endogenous SGOL1 signals at the centromere decreased in the SGOL1-P1-expressing cells (Figure 4b), where the metaphasic chromosomes had a defective alignment as shown in Figure 2. Because SGOL1 prevents cohesin from precocious cleavage at the centromere, we investigated whether RAD21/SCC1, a cohesin subunit, was localized at the centromere. The signals of RAD21 at the centromere also decreased in the SGOL1-P1-expressing cells with the alignment defect (Figure 4c), whereas the signals of PP2A-B56α, a regulatory subunit of the PP2A complex, did not (Figure 4d). These results show that SGOL1-P1 inhibits the localization of native SGOL1 and RAD21 to the centromere, independently of PP2A.

Cohesion defects between sister chromatids in cells expressing SGOL1-P1

The result that RAD21 decreased at the centromere in SGOL1-P1-expressing cells reminded us that cohesion

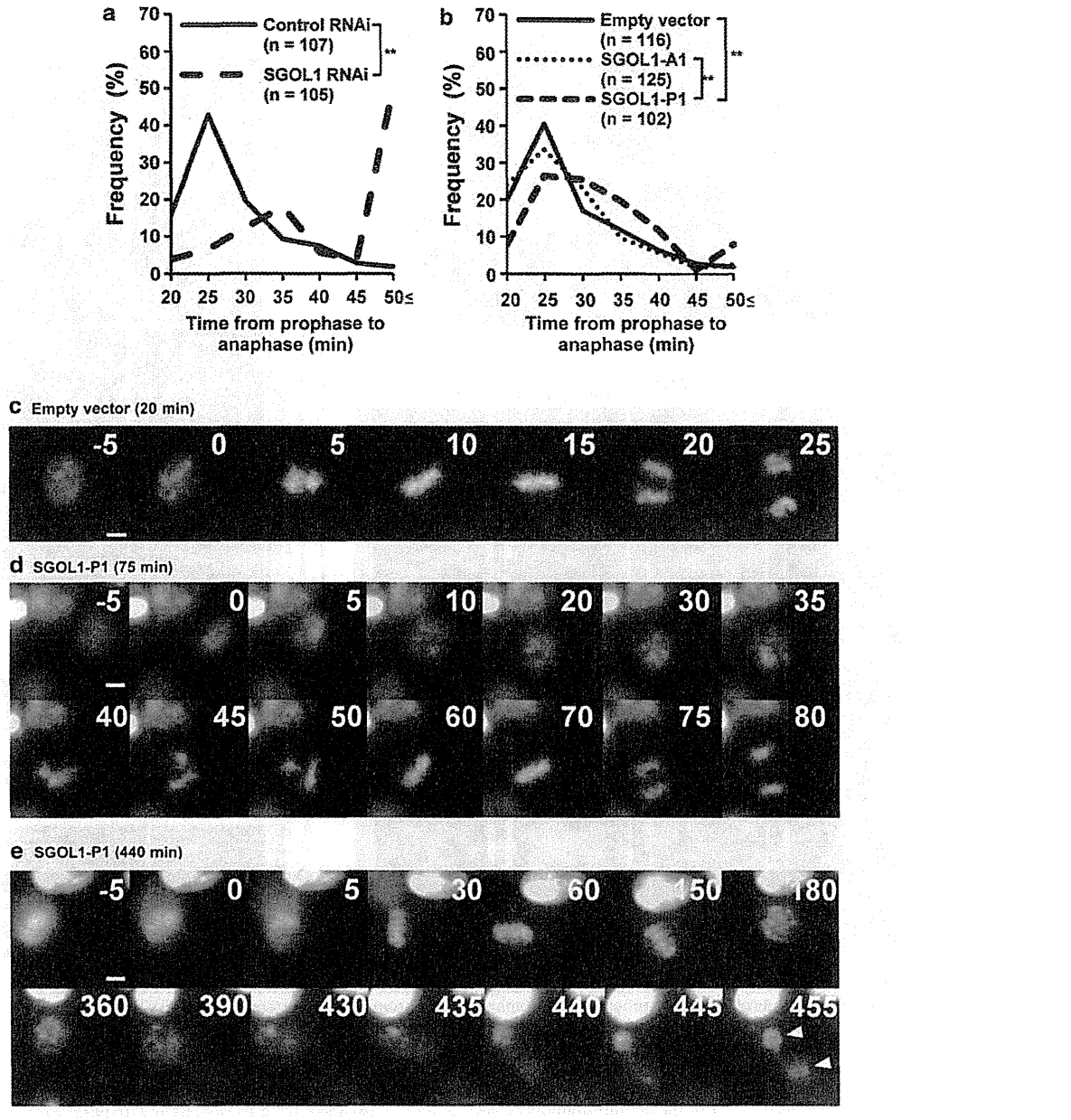

Figure 3 Delayed mitotic progression in cells expressing SGOL1-P1. (**a**, **b**) GFP-histone H2B was co-transfected with pSilencer-SGOL1 or myc-SGOL1, and time-lapse images of the cells were taken at 5 min intervals. The graphs indicate frequency of progression times from nuclear envelope breakdown or chromatin condensation (prophase) to the onset of chromosome-to-pole movement (anaphase). Total cell counts are shown in the graphs. (**c**–**e**) Representative montage images of normal mitotic progression (**c**), delayed progression (**d**, **e**) and abnormal chromosome segregation with immature congression at the metaphase plate (**e**). Arrowheads indicate daughter nuclei. Time in minutes is shown at the upper right of each panel. Scale bar = 5 μm. $^{**}P<0.01$ (χ^2-test).

defect between sister chromatids occurred. To assess the effect of SGOL1-P1 on sister chromatid cohesion, a chromosome spread assay was performed. Spread chromosomes were stained with DAPI (Figure 5a) and the frequency of the each of the separation patterns was counted (Figure 5b). The SGOL1-knockdown cells exhibited a high frequency of severe cohesion defects between sister chromatids, the same as described previously (Tang *et al*., 2004; Kitajima *et al*., 2005; McGuinness *et al*., 2005). Severe cohesion defects were also observed in 11% of the SGOL1-P1-expressing cells, but they were rarely found in the control cells. Cells defecting cohesion between sister chromatids are prone to develop CIN as a result of failure of mitotic progression. Because HCT116 cells have a relatively stable karyotype (45 chromosomes; Kienitz *et al*., 2005), the total number of chromosomes per cluster can be counted. The frequency of the aberrant phenotype, which we defined as a cluster composed of more than 50 chromosomes, was significantly higher in the

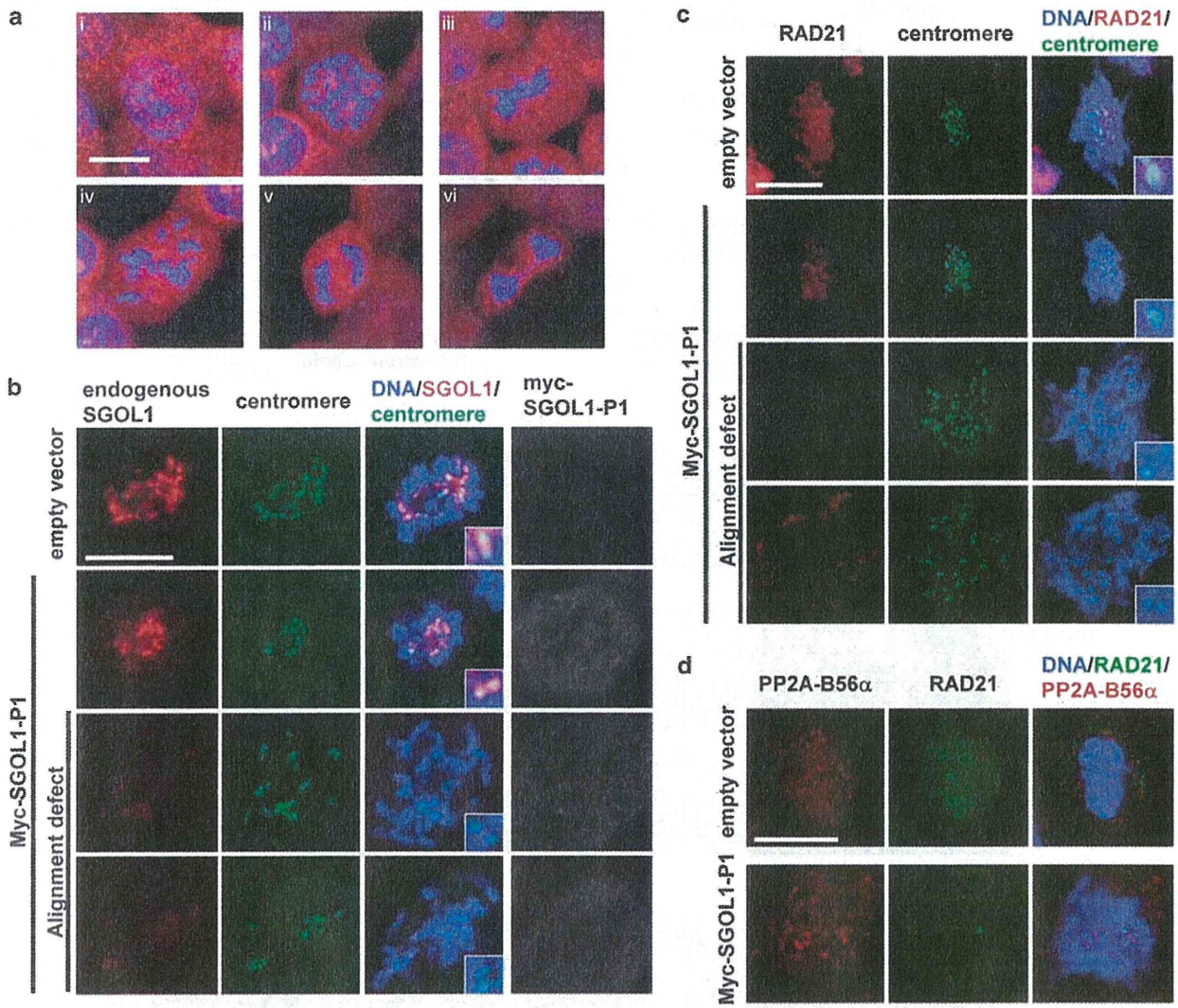

Figure 4 Decrease in centromeric localization of endogenous SGOL1 in cells expressing SGOL1-P1. (**a**) Localization of SGOL1-P1 during the cell cycle. Interphase (I), prophase (II), metaphase (III), chromosomal alignment defect (IV), anaphase (V) and abnormal segregation (VI) are shown with the staining of myc-SGOL1-P1 (red) and DNA (blue). (**b**) Localization of endogenous SGOL1 in cells expressing SGOL1-P1. HCT116 cells were transfected with myc-SGOL1-P1. Following culture with an antibiotic, the cells were fixed with paraformaldehyde (**a**, **b**). Endogenous SGOL1 and myc-SGOL1-P1 were detected using immunofluorescence with mouse anti-hSgo1 and rabbit anti-myc antibodies, respectively. (**c**, **d**) Localization of endogenous RAD21 and PP2A-B56α on chromosomes in cells expressing SGOL1-P1. For the immunostaining of RAD21 and PP2A-B56α, the cells were fixed with paraformaldehyde, followed by spinning down on a glass coverslip and pre-extraction with a detergent. The centromere was detected using immunofluorescence with human anti-centromere autoantibody (**b**, **c**). The inset is a magnified image of the centromere. Scale bar = 10 μm.

SGOL1-knockdown cells ($P = 0.037$, Fisher's exact test), and the frequency of the phenotype tended to be higher in the SGOL1-P1-expressing cells than in the control cells ($P = 0.097$) (Figures 5c and d). These results mean that SGOL1-P1 participates in the precocious separation of sister chromatids and is capable of inducing CIN in the process of cell proliferation.

Abnormal cell phenotypes in the stable cell lines expressing SGOL1-P1

To examine the effects of SGOL1-P1 expression during long-term culture, we established cell lines stably expressing SGOL1-P1 (P3-2 and P4-1) from HCT116 cells (Figure 6a). These cell lines exhibited a slightly higher mitotic frequency, particularly in prometaphase/metaphase, than the parental cell and the stable cell line transfected with the empty vector (Table 1 and Figure 6b). They were also observed to exhibit delayed mitotic progression (Supplementary Figure S5a) and chromosome separation without congression at the metaphase plate when examined by time-lapse fluorescence microscopy (Table 1, Supplementary Figure S5b and Supplementary Movies 3 and 4). The delayed mitotic progression is consistent with the mitotic frequency data. The time-lapse data also indicated that P3-2 and P4-1 have the same properties during mitosis as cells that transiently express SGOL1-P1.

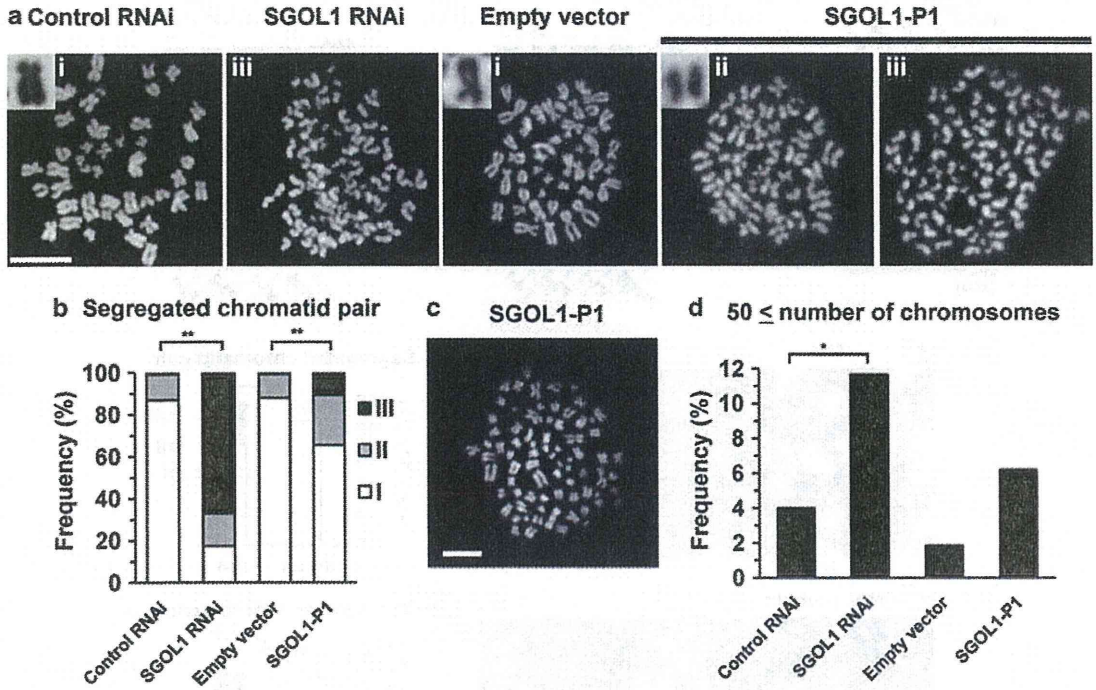

Figure 5 Cohesion defects between sister chromatids in cells expressing SGOL1-P1. (**a**) Representative images of chromosome spread. Transfected HCT116 cells were treated with 100 nM nocodazole for 18 h to arrest the cell cycle during mitosis. Spread chromosomes stained with DAPI were classified into the following three patterns: (I) normal cohesive chromatids or only a very few pairs of separated sister chromatids; (II) separated chromatids have remained in close proximity to the pair partner (several chromatid pairs remain cohesive); and (III) severely separated chromatids (the pair partner is often hard to identify, because it is located some distance away). A representative image of the chromatid pairs exhibiting patterns I and II is inverted and magnified in the left top panel. (**b**) Frequency of cells with cohesion defects between sister chromatids. (**c**) A representative image of a phenotype with an increased number of chromosomes (78 chromosomes). (**d**) The graph shows the frequency of 50 or more chromosomes. Total cell number: Control RNAi, 100; SGOL1 RNAi, 103; empty vector, 108; SGOL1-P1, 113. Scale bar = 10 μm. $*P<0.05$ (Fisher's exact test), $**P<0.01$ (χ^2-test).

Abnormal nuclear shape is known to reflect CIN and to be frequently observed in malignant tumors (Gisselsson *et al.*, 2001). The stable cell lines expressing SGOL1-P1 exhibited less circularity and more frequent micronuclei (Table 1 and Figures 6c and d). We examined cells for the presence of an extra centrosome, because multiple spindle poles have been reported to be common in mitotic SGOL1-knockdown cells (Kitajima *et al.*, 2006; Dai *et al.*, 2009). An extra centrosome was observed more frequently in the cell lines expressing SGOL1-P1 (Table 1 and Figure 6e). Triple daughter nuclei, caused by multiple spindle formation, were also observed almost exclusively in cells expressing SGOL1-P1 (Supplementary Figure S5c and Supplementary Movie 5). We suspected that the culture time of several days shown in Figure 5d was not long enough to induce a full-blown aberrant phenotype in the SGOL1-P1-expressing cells. The increased number of chromosomes mentioned here reflects the aberrant distribution of chromosomes preceding mitosis. Thus, a shorter culture time may not yield sufficient chromosome aberrations from the previous mitosis. Therefore, we examined the number of chromosomes in SGOL1-P1-stably expressing cells, which had passed through more mitotic phases. In addition to the premature separation of sister chromatids, an aberrant number of chromosomes was observed more frequently in cells expressing SGOL1-P1 than in the parent cells (Figures 6f and g). These results indicate that long-term expression of SGOL1-P1 affects nuclear shape, centrosome stability and CIN.

Discussion

SGOL1-P1 was identified as a novel tumor-specific variant and the *SGOL1-P1*-positive tumors were smaller than the *SGOL1-P1*-negative tumors. Because the outcome of the *SGOL1-P1*-positive cases is still unknown, the relationship between *SGOL1-P1* expression and the prognosis remains unclear. As our observations in this study showed that SGOL1-P1 expression induced the HCT116 aberrant karyotype, abnormal nuclear shapes and micronuclei, all of which are indicative of the highly malignant nature of the tumor cells, SGOL1-P1 may drive early stage tumors toward a more aggressive phenotype. After SGOL1-P1 has driven a small benign tumor to undergo malignant transformation, it may not be required for tumor progression. *SGOL1-P1* would rarely be observed in an advanced tumor. This model, in which SGOL1-P1 causes malignancy in the early stage of colon cancer, may be applicable to other types of cancer because *SGOL1-P1* was also detected in lung cancer (Supplementary Figure S6). Comprehensive analysis of the role of SGOL1-P1 is now under way in lung cancer.

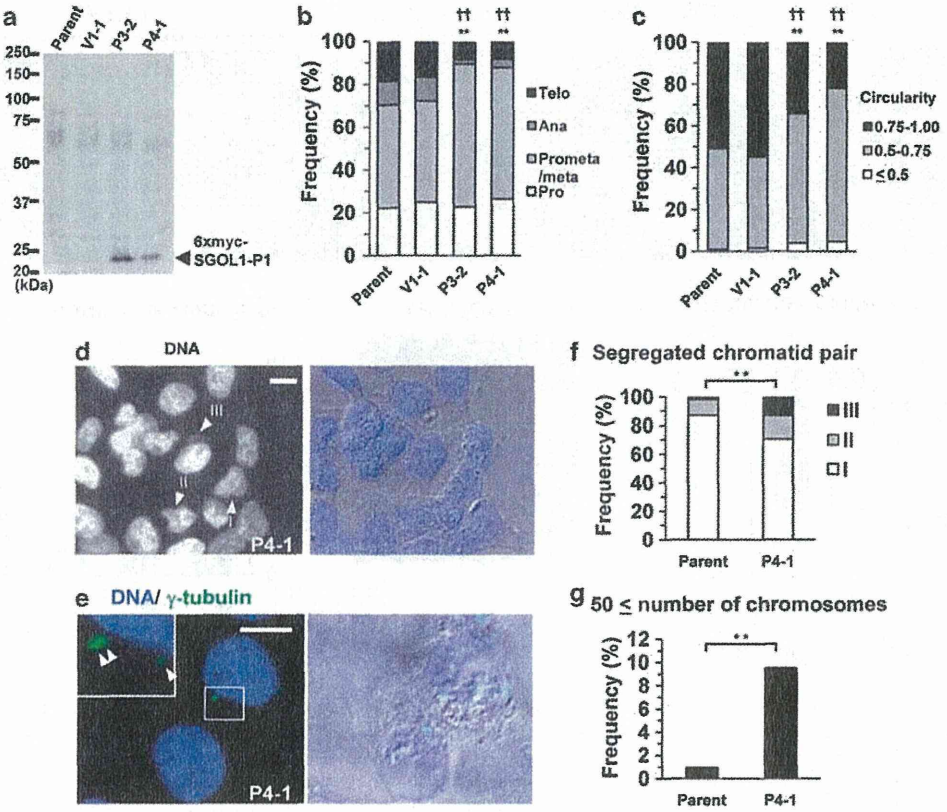

Figure 6 Aberrant cell phenotypes and mitotic progression in cells constitutively expressing SGOL1-P1. (**a**) Stable cell lines were produced from HCT116 cells. P3-2 and P4-1 are the cell lines expressing myc-SGOL1-P1, whereas V1-1 is a cell line derived from the cells transfected with empty vector. Anti-myc antibody was used for the immunoblotting. (**b–d**) The stable cell lines and parental cells were stained with DAPI. The graph shows the frequency of each mitotic phase (**b**). Nuclear circularity was calculated by using the formula: $4\pi \times A/p^2$ (A = area, p = perimeter) (**c**). Representative distorted nuclei (arrowheads 'I' and 'II') and a micronucleus ('III') are shown (**d**). (**e**) Immunofluorescence staining was performed with anti-γ-tubulin antibody. A magnified image is shown in the left top panel. Arrowheads indicate centrosomes. The panel on the right is a merged image of DNA (blue) and differential interference contrast (gray). (**f, g**) Chromosome spread assay was performed with P4-1 and parent cells as described in Figure 5. Total cell numbers: Parent, 1027 (**b**), 418 (**c**) and 106 (**f, g**); V1-1, 1130 (**b**) and 441 (**c**); P3-2, 1106 (**b**) and 452 (**c**); P4-1, 1152 (**b**), 403 (**c**) and 105 (**f, g**). Scale bar = 10 μm. $^{**}P<0.01$ vs parent, $^{\dagger\dagger}P<0.01$ vs V1-1 (χ^2-test). Fisher's exact test was also used (**g**).

Table 1 Aberrant cell phenotypes and mitotic progression in cells that constitutively expressed SGOL1-P1

	Fixed cells			*Living cells*
	Micronucleus[a] *frequency (%)*	*Extra centrosome*[a] *frequency (%)*	*Mitotic index frequency (%)*	*Immature metaphase*[b] *frequency (%)*
Parent	4/418 (0.96)	1/266 (0.38)	27/1027 (2.63)	0/174 (0.00)
V1-1	5/441 (1.13)	1/282 (0.35)	36/1130 (3.19)	0/158 (0.00)
P3-2	9/452 (1.99)	5/279 (1.79)	48/1106 (4.34)**,†	6/170 (3.53)*,†
P4-1	16/403 (3.97)**,†	8/247 (3.24)*,†	49/1152 (4.25)**,††	13/159 (8.18)**,††

[a]Refer to Figure 6.
[b]Chromosomal mass, separated without metaphase congression or after congression, too brief to be observed in images acquired at 5-min intervals. Statistical analyses were performed by using the χ^2-test for the mitotic index data and Fisher's exact test for other data.
$^{*}P<0.05$ vs parent, $^{\dagger}P<0.05$ vs V1-1, $^{**}P<0.01$ vs parent and $^{\dagger\dagger}P<0.01$ vs V1-1.

The concept that tumors are composed of a heterogeneous population of cells has been established (Reya *et al.*, 2001). Cancer stem cells (CSCs) exhibit both properties of self-renewal and differentiation into diverse cancer cell types and they are thought to be responsible for tumors being composed of a heterogeneous population of cells. When chromosomal abnormalities occur in CSCs, the phenotypic diversity of the cells in a tumor may increase and have a negative impact on the outcome, because of the acquisition of malignant properties, such as drug resistance and metastasis. Therefore, it is also expected that shugoshin studies will be performed in the field of CSCs in order to investigate its impact on tumor progression.

Aberrant chromosome alignment at the metaphase plate is thought to be due to unstable chromatid cohesion. It has

recently been reported that a mono-oriented chromosome is transported toward the metaphase plate along the kinetochore fiber that has already attached to the bi-oriented chromosomes remaining at the metaphase plate (Kapoor *et al.*, 2006), and that cohesion between chromatids at the centromere influences kinetochore geometry and determines kinetochore orientation (Sakuno *et al.*, 2009). Therefore, inappropriate kinetochore orientation is thought to cause the defect in transport to the metaphase plate and result in the aberrant chromosome alignment in cells expressing SGOL1-P1.

The number of cells that contained an extra centrosome increased in the presence of SGOL1-P1 in our experiment. This finding was consistent with the results of a previous study in which spindle pole integrity was found to require chromosome cohesion (Dai *et al.*, 2009). In that study, knockdown of haspin, SGOL1 or RAD21, all of which are necessary for chromosome cohesion, resulted in an increase in the number of γ-tubulin foci. Thus, the overexpression of SGOL1-P1 should also impair centrosome stability by interfering with chromatid cohesion.

This is the first study to report an association between cancer and a SGOL1 variant. As SGOL1-P1 expression inhibited the localization of endogenous SGOL1 and RAD21 to the centromere in our experiments, SGOL1-P1 is thought to function as a negative factor to native SGOL1. Although the details of the molecular mechanism mediated by SGOL1-P1 remain unclear, a protein–protein interaction with an, as yet, unidentified protein is assumed to be involved in the mechanism. SGOL1-P1 is composed of 59 amino acids, and the region of SGOL1-A1 protein (amino acids 1–47) encoded by exon 1 and exon 2 of the *SGOL1* gene accounts for 79.7% of the amino acid sequence of SGOL1-P1. Having the amino acid sequence 51–96 is sufficient for SGOL1 to bind PP2A (Xu *et al.*, 2009). This amino acid region is within the exon 3-coded region (aa 48–113), and SGOL1 mutant N61I actually does not exhibit binding activity to PP2A (Tang *et al.*, 1998, 2006; Xu *et al.*, 2009). Thus, PP2A is probably not a target of SGOL1-P1. Actually, the localization of PP2A-B56α on chromosomes was not affected by SGOL1-P1 expression, even in cells with a reduction in RAD21 signals. Similarly, heterochromatin protein HP1α, a SGOL1-interacting protein that is required for localization and functioning of SGOL1 at the centromere does not seem to be a target either, because the binding region of SGOL1 to HP1α is located in the C-terminal area (Yamagishi *et al.*, 2008). As it is more likely that SGOL1-P1 inhibits the interaction between native SGOL1 and as yet unidentified targets, we are currently searching for proteins that interact with SGOL1-P1.

There is also the possibility that the SGOL1-P1-unique sequence may be involved in abnormal chromosome alignment. The C-terminal short region of SGOL1-P1 corresponds to exon 4 in the frameshift and this frameshift is what makes the SGOL1-P1 sequence unique among SGOL1 variants. Interestingly, a BLAST search of the NCBI's protein database revealed that the C-terminal unique sequence of SGOL1-P1 is similar to the conserved region of the Polo-like kinase (Plk) family. The part of the sequence in the Plk family proteins that is similar to the C-terminal unique sequence of SGOL1-P1 and the adjacent residues are conserved among species and form a catalytic loop (Supplementary Figure S7; Kothe *et al.*, 2007). The results of the NCBI's Conserved Domains Database search also suggested that the Plk1 catalytic loop includes ATP- and substrate-binding sites (accession number cd05123), and thus SGOL1-P1 may interfere with Plk1-mediated phosphorylation through the conserved region described above. If this model, in which SGOL1-P1 targets Plk1, is correct, the abnormal chromosome alignment and the precociously separated chromatids found in the SGOL1-P1-expressing cells should be independent of each other, because Plk1 is required for assembly of the mitotic spindle, but not for chromatid cohesion (Losada *et al.*, 2002; Sumara *et al.*, 2002, 2004; Eot-Houllier *et al.*, 2008). The spatio-temporal function of SGOL1-P1 in relation to Plk1 and native SGOL1 may cause the abnormal mitotic phenotypes observed in the present study.

The results of the present study demonstrated an association between SGOL1-P1 and colon cancer, and they suggest that native SGOL1 is deregulated by SGOL1-P1. Further studies, such as studies of SGOL1-P1 expression in other types of cancer, of the mechanism of generation of SGOL1-P1 transcripts and of the molecular targets of SGOL1-P1, should improve our understanding of how tumors are generated and become malignant.

Materials and methods

RT–PCR and plasmid construction

RT–PCR was carried out as described in our previous report (Iwaizumi *et al.*, 2009). The primer sequences used for the first RT–PCR (Figure 1b) were 5′-GGAGGAGGAAGATAG CTGTTGC-3′ (sense) and 5′-TATGGCAATGGCTCACTC TG-3′ (antisense). The PCR products from non-tumor tissue and tumor tissue were cloned and used for the sequence analysis. A primer targeting the junction between exon 2 and exon 4 was constructed for routine detection of *SGOL1-P1* transcripts in specimens (Supplementary Figure S1). Glyceraldehyde-3-phosphate dehydrogenase (GAPDH) was amplified as an internal control, and the quantitative real-time RT–PCR was carried out as described previously (Iwaizumi *et al.*, 2009). To express SGOL1-P1 in mammalian cells, six myc tags were fused to the N-terminus of SGOL1-P1 and the product was inserted into pcDNA3.1. The pSilencer plasmid with short hairpin RNA (shRNA) targeting the SGOL1 sequence was used for the RNA interference (RNAi) procedure as described previously (Iwaizumi *et al.*, 2009).

Cell culture and transfection

Human colon cancer cell line HCT116 was cultured at 37 °C in RPMI medium (Invitrogen, Carlsbad, CA, USA) containing 10% fetal bovine serum (Nichirei, Tokyo, Japan), under 5% CO_2. Transfection was performed by using Lipofectamine 2000 (Invitrogen) according to the manufacturer's protocol. Stable cell lines expressing myc-SGOL1 (A1 or P1) were generated by incubating the transfected cells in selection medium containing 200 μg/ml geneticin (Invitrogen) and

performing limiting-dilution cloning. Cells subcultured for 25–45 passages were used in the experiments.

Antibodies
Rabbit polyclonal anti-shugosin (ab21633; Abcam, Cambridge, MA, USA; Figure 2c), anti-myc tag (06-549; Millipore, Bedford, MA, USA) and anti-Rad21 antibodies (ab992; Abcam; Figure 4d), mouse polyclonal anti-PPP2R5A antibodies (PP2A-B56α) (H00005525-B01P; Abnova, Taipei, Taiwan) and mouse monoclonal anti-β-tubulin (2-28-33; Sigma, St Louis, MO, USA), anti-hSgo1 (Figure 4b), and anti-Rad21 (53A303; Millipore; Figure 4c) and anti-γ-tubulin antibodies (GTU88; Sigma) were used for immunoblotting and immunofluorescence staining. Human autoantibody against the centromere (Immunovison, Springdale, AR, USA) was used for immunofluorescence staining of kinetochore. HRP-conjugated donkey polyclonal anti-rabbit antibody or anti-mouse IgG antibody (GE Healthcare, Piscataway, NJ, USA) and Alexa Fluor 488/546/633-conjugated goat polyclonal anti-rabbit, anti-mouse or anti-human IgG antibodies (Invitrogen) were used as secondary antibodies.

Immunoblotting
Immunoblotting was performed as described previously (Kahyo *et al*., 2008). Briefly, the protein concentration of the lysate was measured with a BCA protein assay kit (Thermo Scientific, Rockford, IL, USA). Following the addition of SDS sample buffer, the samples were boiled at 95 °C for 5 min and they were then subjected to SDS–polyacrylamide gel electrophoresis. Cell lysate of 10 μg was loaded on the gel.

Confocal laser scanning
Cells plated on fibronectin-coated glass coverslips (Becton Dickinson, Franklin Lakes, NJ, USA) were transfected with myc-SGOL1 or shRNA of SGOL1 and cultured for 24 h. The cells were cultured in presence of puromycin (0.8 μg/ml, Sigma) for RNAi or geneticin (200 μg/ml) for the expression assay. After culture for 48 h, they were fixed with 4% paraformaldehyde in phosphate-buffered saline (PBS) buffer (140 mM NaCl, 2.7 mM KCl, 8.1 mM sodium phosphate dibasic and 1.5 mM potassium phosphate monobasic) at room temperature for 15 min, permealized with 0.1% Triton X-100 and subjected to immunostaining. For γ-tubulin, staining cells were fixed with cold methanol at −20 °C for 5 min. To detect RAD21 and PP2A-B56α signals on the chromosomes clearly, we referred to previous reports (Waizenegger *et al*., 2000; Kitajima *et al*., 2006; Lee *et al*., 2008). Briefly, cultured cells were spun on a glass coverslip for 5 min at 290 *g* and pre-treated with 0.1% Triton X-100 in PBS at room temperature for 2 min before fixation with 4% paraformaldehyde. All of the cells were stained with 1.5 μg/ml 4′,6-diamidine-2-phenylindole (DAPI, Invitrogen) to visualize their nuclei. Fluorescence signals were detected by confocal laser scanning microscopy (FV1000; Olympus, Tokyo, Japan). The lengths of horizontal and vertical axes were measured with Image J software (version 1.43f; National Institutes of Health, Bethesda, MD, USA).

Chromosome spread
Transfected cells were selected with antibiotics as described above. After culture for 48 h, the cells were treated with 100 nM nocodazole (Sigma) for 18 h. They were then trypsinized and collected by centrifugation in a conical tube. The cells were gently suspended with hypotonic solution (75 mM KCl) and incubated at 37 °C for 6 min. Chilled fixative solution (methanol:glacial acetic acid, 3:1) was gently added to the cells that had been collected by centrifugation, and this procedure consisting of centrifugation, collection of the cells and addition of chilled fixative solution was repeated three times. The fixed cells were dropped onto the slide glasses. After drying in air, they were stained with DAPI.

Time-lapse imaging
Myc-SGOL1 and GFP-Histone H2B plasmids were used to co-transfect HCT116 cells plated on the fibronectin-coated glass-bottom dishes, and 48 h later, the medium was replaced with fresh medium and the cells were subjected to time-lapse imaging (FCV100; Olympus). Fluorescence signals from GFP were captured at 5 min intervals for 24 h and the data were used to prepare the montage images and movies.

Statistical analysis
The Mann–Whitney *U*-test was used to statistically analyze non-parametric data. The χ^2-test or Fisher's exact test was used to compare categorical variables. The statistical analysis was performed by using the Microsoft Excel software program (Microsoft, Redman, WA, USA).

Ethics
The design of this study, including the human genomics and recombinant DNA research, was approved by the Institutional Review Board of Hamamatsu University School of Medicine.

Conflict of interest

The authors declare no conflict of interest.

Acknowledgements

We thank Dr Suzuki of The Jikei University School of Medicine for providing the anti-hSgo1 antibody. This work was supported by a Grant-in-Aid for Scientific Research (C) (22590356) and for priority areas (20014007 and 221S0001) from the Japanese Ministry of Education, Culture, Sports, Science and Technology, Grants-in-Aid for the 3rd Term Comprehensive 10-Year-Strategy for Cancer Control and Grants-in-Aid for Cancer Research from the Japanese Ministry of Health (21-1) and from the Smoking Research Foundation.

References

Bharadwaj R, Yu H. (2004). The spindle checkpoint, aneuploidy, and cancer. *Oncogene* **23**: 2016–2027.

Clift D, Bizzari F, Marston AL. (2009). Shugoshin prevents cohesin cleavage by PP2A(Cdc55)-dependent inhibition of separase. *Genes Dev* **23**: 766–780.

Dai J, Kateneva AV, Higgins JM. (2009). Studies of haspin-depleted cells reveal that spindle-pole integrity in mitosis requires chromosome cohesion. *J Cell Sci* **122**: 4168–4176.

Eot-Houllier G, Fulcrand G, Watanabe Y, Magnaghi-Jaulin L, Jaulin C. (2008). Histone deacetylase 3 is required for centromeric

H3K4 deacetylation and sister chromatid cohesion. *Genes Dev* **22**: 2639–2644.

Gisselsson D, Bjork J, Hoglund M, Mertens F, Dal Cin P, Akerman M *et al.* (2001). Abnormal nuclear shape in solid tumors reflects mitotic instability. *Am J Pathol* **158**: 199–206.

Goldstein LS. (1980). Mechanisms of chromosome orientation revealed by two meiotic mutants in Drosophila melanogaster. *Chromosoma* **78**: 79–111.

Grady WM. (2004). Genomic instability and colon cancer. *Cancer Metastasis Rev* **23**: 11–27.

Hauf S, Waizenegger IC, Peters JM. (2001). Cohesin cleavage by separase required for anaphase and cytokinesis in human cells. *Science* **293**: 1320–1323.

Iwaizumi M, Shinmura K, Mori H, Yamada H, Suzuki M, Kitayama Y *et al.* (2009). Human Sgo1 downregulation leads to chromosomal instability in colorectal cancer. *Gut* **58**: 249–260.

Kahyo T, Mostoslavsky R, Goto M, Setou M. (2008). Sirtuin-mediated deacetylation pathway stabilizes Werner syndrome protein. *FEBS Lett* **582**: 2479–2483.

Kanda T, Sullivan KF, Wahl GM. (1998). Histone-GFP fusion protein enables sensitive analysis of chromosome dynamics in living mammalian cells. *Curr Biol* **8**: 377–385.

Kapoor TM, Lampson MA, Hergert P, Cameron L, Cimini D, Salmon ED *et al.* (2006). Chromosomes can congress to the metaphase plate before biorientation. *Science* **311**: 388–391.

Karamysheva Z, Diaz-Martinez LA, Crow SE, Li B, Yu H. (2009). Multiple anaphase-promoting complex/cyclosome degrons mediate the degradation of human Sgo1. *J Biol Chem* **284**: 1772–1780.

Kawashima SA, Yamagishi Y, Honda T, Ishiguro K, Watanabe Y. (2010). Phosphorylation of H2A by Bub1 prevents chromosomal instability through localizing shugoshin. *Science* **327**: 172–177.

Kerrebrock AW, Moore DP, Wu JS, Orr-Weaver TL. (1995). Mei-S332, a Drosophila protein required for sister-chromatid cohesion, can localize to meiotic centromere regions. *Cell* **83**: 247–256.

Kienitz A, Vogel C, Morales I, Muller R, Bastians H. (2005). Partial downregulation of MAD1 causes spindle checkpoint inactivation and aneuploidy, but does not confer resistance towards taxol. *Oncogene* **24**: 4301–4310.

Kitajima TS, Hauf S, Ohsugi M, Yamamoto T, Watanabe Y. (2005). Human Bub1 defines the persistent cohesion site along the mitotic chromosome by affecting Shugoshin localization. *Curr Biol* **15**: 353–359.

Kitajima TS, Kawashima SA, Watanabe Y. (2004). The conserved kinetochore protein shugoshin protects centromeric cohesion during meiosis. *Nature* **427**: 510–517.

Kitajima TS, Sakuno T, Ishiguro K, Iemura S, Natsume T, Kawashima SA *et al.* (2006). Shugoshin collaborates with protein phosphatase 2A to protect cohesin. *Nature* **441**: 46–52.

Kothe M, Kohls D, Low S, Coli R, Cheng AC, Jacques SL *et al.* (2007). Structure of the catalytic domain of human polo-like kinase 1. *Biochemistry* **46**: 5960–5971.

Lee J, Kitajima TS, Tanno Y, Yoshida K, Morita T, Miyano T *et al.* (2008). Unified mode of centromeric protection by shugoshin in mammalian oocytes and somatic cells. *Nat Cell Biol* **10**: 42–52.

Lengauer C, Kinzler KW, Vogelstein B. (1998). Genetic instabilities in human cancers. *Nature* **396**: 643–649.

Losada A, Hirano M, Hirano T. (2002). Cohesin release is required for sister chromatid resolution, but not for condensin-mediated compaction, at the onset of mitosis. *Genes Dev* **16**: 3004–3016.

Lupas A, Van Dyke M, Stock J. (1991). Predicting coiled coils from protein sequences. *Science* **252**: 1162–1164.

Marston AL, Tham WH, Shah H, Amon A. (2004). A genome-wide screen identifies genes required for centromeric cohesion. *Science* **303**: 1367–1370.

Mayr C, Bartel DP. (2009). Widespread shortening of 3′UTRs by alternative cleavage and polyadenylation activates oncogenes in cancer cells. *Cell* **138**: 673–684.

McGuinness BE, Hirota T, Kudo NR, Peters JM, Nasmyth K. (2005). Shugoshin prevents dissociation of cohesin from centromeres during mitosis in vertebrate cells. *PLoS Biol* **3**: e86.

Moore DP, Page AW, Tang TT, Kerrebrock AW, Orr-Weaver TL. (1998). The cohesion protein MEI-S332 localizes to condensed meiotic and mitotic centromeres until sister chromatids separate. *J Cell Biol* **140**: 1003–1012.

Nasmyth K, Peters JM, Uhlmann F. (2000). Splitting the chromosome: cutting the ties that bind sister chromatids. *Science* **288**: 1379–1385.

Peters JM. (2002). The anaphase-promoting complex: proteolysis in mitosis and beyond. *Mol Cell* **9**: 931–943.

Pihan GA, Doxsey SJ. (1999). The mitotic machinery as a source of genetic instability in cancer. *Semin Cancer Biol* **9**: 289–302.

Rabitsch KP, Gregan J, Schleiffer A, Javerzat JP, Eisenhaber F, Nasmyth K. (2004). Two fission yeast homologs of Drosophila Mei-S332 are required for chromosome segregation during meiosis I and II. *Curr Biol* **14**: 287–301.

Rajagopalan H, Lengauer C. (2004). Aneuploidy and cancer. *Nature* **432**: 338–341.

Reya T, Morrison SJ, Clarke MF, Weissman IL. (2001). Stem cells, cancer, and cancer stem cells. *Nature* **414**: 105–111.

Riedel CG, Katis VL, Katou Y, Mori S, Itoh T, Helmhart W *et al.* (2006). Protein phosphatase 2A protects centromeric sister chromatid cohesion during meiosis I. *Nature* **441**: 53–61.

Sakuno T, Tada K, Watanabe Y. (2009). Kinetochore geometry defined by cohesion within the centromere. *Nature* **458**: 852–858.

Salic A, Waters JC, Mitchison TJ. (2004). Vertebrate shugoshin links sister centromere cohesion and kinetochore microtubule stability in mitosis. *Cell* **118**: 567–578.

Shinmura K, Iwaizumi M, Igarashi H, Nagura K, Yamada H, Suzuki M *et al.* (2008). Induction of centrosome amplification and chromosome instability in p53-deficient lung cancer cells exposed to benzo[a]pyrene diol epoxide (B[a]PDE). *J Pathol* **216**: 365–374.

Sumara I, Gimenez-Abian JF, Gerlich D, Hirota T, Kraft C, de la Torre C *et al.* (2004). Roles of polo-like kinase 1 in the assembly of functional mitotic spindles. *Curr Biol* **14**: 1712–1722.

Sumara I, Vorlaufer E, Stukenberg PT, Kelm O, Redemann N, Nigg EA *et al.* (2002). The dissociation of cohesin from chromosomes in prophase is regulated by Polo-like kinase. *Mol Cell* **9**: 515–525.

Suzuki H, Akiyama N, Tsuji M, Ohashi T, Saito S, Eto Y. (2006). Human Shugoshin mediates kinetochore-driven formation of kinetochore microtubules. *Cell Cycle* **5**: 1094–1101.

Tang TT, Bickel SE, Young LM, Orr-Weaver TL. (1998). Maintenance of sister-chromatid cohesion at the centromere by the Drosophila MEI-S332 protein. *Genes Dev* **12**: 3843–3856.

Tang Z, Shu H, Qi W, Mahmood NA, Mumby MC, Yu H. (2006). PP2A is required for centromeric localization of Sgo1 and proper chromosome segregation. *Dev Cell* **10**: 575–585.

Tang Z, Sun Y, Harley SE, Zou H, Yu H. (2004). Human Bub1 protects centromeric sister-chromatid cohesion through Shugoshin during mitosis. *Proc Natl Acad Sci USA* **101**: 18012–18017.

Waizenegger IC, Hauf S, Meinke A, Peters JM. (2000). Two distinct pathways remove mammalian cohesin from chromosome arms in prophase and from centromeres in anaphase. *Cell* **103**: 399–410.

Wasch R, Robbins JA, Cross FR. (2010). The emerging role of APC/CCdh1 in controlling differentiation, genomic stability and tumor suppression. *Oncogene* **29**: 1–10.

Xu Z, Cetin B, Anger M, Cho US, Helmhart W, Nasmyth K *et al.* (2009). Structure and function of the PP2A-shugoshin interaction. *Mol Cell* **35**: 426–441.

Yamagishi Y, Sakuno T, Shimura M, Watanabe Y. (2008). Heterochromatin links to centromeric protection by recruiting shugoshin. *Nature* **455**: 251–255.

Supplementary Information accompanies the paper on the Oncogene website (http://www.nature.com/onc)

Journal of Human Genetics (2012) 00, 1–6

www.nature.com/jhg

ORIGINAL ARTICLE

Association between dopamine beta hydroxylase rs5320 polymorphism and smoking behaviour in elderly Japanese

Elakeche Ella[1,2], Naomi Sato[2,3], Daisuke Nishizawa[4], Shinji Kageyama[2], Hidetaka Yamada[1], Nobuya Kurabe[2], Keiko Ishino[2], Hong Tao[2], Fumihiko Tanioka[5], Akiko Nozawa[3], Chen Renyin[2,6], Kazuya Shinmura[2], Kazutaka Ikeda[4] and Haruhiko Sugimura[2]

The dopaminergic brain pathway is involved in many addictive behaviours, hence represents a good candidate in the study of smoking behaviour and nicotine addiction. Dopamine beta hydroxylase (DBH) is an enzyme that catalyses the conversion of dopamine into noradrenaline. This study, the first of its kind, was done to investigate the role of *DBH* rs5320 polymorphism in smoking behaviour of elderly Japanese. This was done by collecting blood samples from 2521 subjects with various smoking habits to genotype the *DBH* rs5320 polymorphism. Participants also had to fill out a questionnaire containing questions regarding their lifestyles. Some of the questions were from the Fagerström Test for Nicotine Dependence (FTND) and the Tobacco Dependence Screener (TDS). It was found that male ever-smokers with AA genotype smoked less cigarettes per day than those with GG and AG genotypes. FTND scores were also lowest in male ever-smokers with AA genotype and in female ever-smokers with AG genotype. There was no correlation detected between the TDS scores and any of the genotypes. This study shows that *DBH* rs5320 polymorphism influences nicotine dependence.
Journal of Human Genetics advance online publication, 19 April 2012; doi:10.1038/jhg.2012.40

Keywords: addiction; dopamine beta hydroxylase (*DBH*); Fagerström Test for Nicotine Dependence (FTND); nicotine dependence; single-nucleotide polymorphism (SNP); smoking behaviour; Tobacco Dependence Screener (TDS)

INTRODUCTION

Dopamine beta hydroxylase (DBH) is an enzyme that catalyses the conversion of dopamine to noradrenaline in sympathetic nerves. DBH is expressed in noradrenaline-containing neurons, occurring in both membrane-bound and soluble forms.[1] Because of this, noradrenaline and DBH are released together during synaptic transmission,[2,3] hence they can be found in cerebrospinal fluid, and plasma or serum. The human gene encoding DBH is located on chromosome 9q34.[4] The *DBH* gene is composed of 12 exons and comprises a sequence of approximately 23 kb.[5] Serum DBH activity of human as well as gorilla have been known to be polymorphic for the last 30 years.[6–9] This inter-individual difference in serum DBH of European population has been stated as being mostly related to a promoter polymorphism at the −1021 promoter region (C to T, rs1611115).[10] Furthermore, there are probably a few pathogenetic germline mutations of *DBH* that explain rare congenital deficiency. The amino-acid substitutions from Asparaginate to Glutaminate at codon 100 in the exon 2 of DBH (300C-A transversion), from Valine to Methionine at codon 87 in the exon 1 of DBG (259 G-A transition) and from Asparaginate to Asparagine at codon 331 in the exon 6 (991 G-A transition) together with splice site mutation (IVS1DS, T-C, +2) are known.[11,12] Clinical phenotypes of these deficiencies are mainly severe orthostatic hypotension and other autonomic nerve symptoms. On the other hand, other polymorphisms also have been investigated in view of a possible modulator of human conditions including psychiatric ones.

In this study, we investigated various aspects of smoking behaviour in relation to single-nucleotide polymorphism in *DBH*. The particular polymorphism investigated was the rs5320, as it was found that the minor allele frequency of this polymorphism existed in substantial number in our Japanese sample. This particular polymorphism has been shown to be associated with Parkinson's disease among North Indians,[13] but our study is the first to investigate its involvement in the role of smoking behaviours.

[1]University of Malta Medical School, Mater Dei Hospital, Tal-Qroqq, Msida MSD, Malta; [2]Department of Tumor Pathology, Hamamatsu University School of Medicine, Hamamatsu, Japan; [3]Department of Clinical Nursing, Hamamatsu University School of Medicine, Hamamatsu, Japan; [4]Research Project for Addictive Substances, Tokyo Metropolitan Institute of Medical Science, Tokyo, Japan; [5]Department of Pathology, Iwata City Hospital, Iwata, Japan and [6]Pathology Department, First Affiliated Hospital of Zhenzhou University, Henan, China
Correspondence: Dr H Sugimura, Department of Tumor Pathology, Hamamatsu University School of Medicine, 1-20-1, Handayama, 431-3192 Hamamatsu, Japan.
E-mail: hsugimur@hama-med.ac.jp
or Dr N Sato, Department of Clinical Nursing, Hamamatsu University School of Medicine, 1-20-1, Handayama, 431-3192 Hamamatsu, Japan.
E-mail: naomi25@hama-med.ac.jp
Received 25 January 2012; revised 6 March 2012; accepted 23 March 2012

MATERIALS AND METHODS

Questionnaire

Blood was collected from 2521 subjects (1616 males and 905 females) between the ages of 60 and 94 years. This was done at the Iwata City Hospital during a 5-year period from 2003 to 2008. The participants involved in this experiment had various smoking habits (1349 male ever-smokers (current-smokers and ex-smokers; 83.5%) and 83 female ever-smokers (9.2%)). To be eligible for this experiment, the participants had to be ambulant and be able to communicate orally. All subjects provided written consent before participating in this study. The overall portraits of subjects have been described previously.[14] The participants were required to fill in a questionnaire leaflet containing various questions about lifestyle, including alcohol consumption, smoking, diet and cancer history. They were assisted in filling out the leaflet by professional interviewers. Some of the questions were from the Fagerström Test for Nicotine Dependence (FTND; a test that yields a continuous measure of nicotine dependence),[15] and Tobacco Dependence Screener (TDS; a screening questionnaire for tobacco/nicotine dependence according to the *International Statistical Classification of Diseases and Related Health Problems* (ICD)-10, *Diagnostic and Statistical Manual of Mental Disorders* (DSM)-III-R and DSM-IV), which consists of 10 questions.[16] The questionnaire also included questions about the numbers of cigarettes smoked per day (CPD), the participants' age when they started smoking, how many times current-smokers had tried to quit smoking and how many times ex-smokers had tried to quit smoking before succeeding.

The study design was approved by the Institutional Review Board of Hamamatsu University School of Medicine.

Genotype analysis

DNA was extracted from the blood samples given by the participants using a QIAamp DNA Blood Maxi kit according to the manufacturers' instructions (Qiagen, Hamburg, Germany). A 50 ng sample of each subjects DNA was amplified by PCR, with the primer set for *DBH* rs5320 polymorphism using the StepOne (Applied BioSystems, Carlsbad, CA, USA). The Assay ID is C_12020332_20. Successful genotyping of *DBH* was performed in 100% of the enrolled subjects. The rate of successful genotyping was almost the same as the other genotype.[17]

Statistical analysis

The genotype of the *DBH* rs5320 polymorphism was tested for Hardy–Weinberg equilibrium using the SPSS statistics software (SPSS Japan, Tokyo, Japan). χ^2 tests of each genotype were performed for smoking status and lung cancer history. The CPD values, FTND scores, TDS scores and trial times for quitting smoking were evaluated according to smoking status and each genotype by the Kruskal–Wallis test or Mann–Whitney *U* test (SPSS Japan).

RESULTS

The age, sex and smoking status of the participants have been reported previously[14] and are shown in Table 1. The age of participants whose DNA could be genotyped ranged from 60 to 94, with the mean age for males being 73.1 years and for females being 73.0 years. Most of the male participants (62%) were ex-smokers, whereas most of the female participants (90.8%) had never smoked. Current-smokers of both sexes had higher TDS than ex-smokers of both sexes. The average CPD for male current-smokers was 16.6 and for female current-smokers 12.2.

Most current-smokers were also current drinkers, and never-smokers of both sexes tended to be never-drinkers ($\chi^2 = 17.7$, $P = 0.001$ for males and $\chi^2 = 42.1$, $P < 0.001$ for females). Table 1 also shows that ex-smokers of both sexes went through more trials to quit smoking than current-smokers.

Table 2 shows that most of the male and female participants had the GG genotype of the *DBH* rs5320 polymorphism ($n = 1275$, 78.9% for males and $n = 693$, 76.6% for females), followed by the AG genotype and finally the AA phenotype (1.4% of males and 1.3% of

Table 1 Subjects profile

Variables	*Males*	P-*value*	*Females*	P-*value*
Number of subjects	1616		905	
Mean age, years (±s.d.)	73.1 (±6.2)		73.0 (±6.4)	
Age distribution, n (%)				
60–64	81 (5.0)		51 (5.6)	
65–69	426 (26.4)		253 (28.0)	
70–74	456 (28.2)		240 (26.5)	
75–79	418 (25.9)		198 (21.9)	
80–84	170 (10.5)		134 (14.8)	
85–89	51 (3.1)		25 (2.8)	
90–	14 (0.9)		4 (0.4)	
Smoking status, n (%)				
Current-smokers	345 (21.3)		30 (3.3)	
Ex-smokers	1004 (62.1)		53 (5.9)	
Never-smokers	267 (16.5)		822 (90.8)	
Mean age according to smoking status, years (±s.d.)				
Current-smokers	72.1 (±6.0)	0.002[a]	70.8 (±5.0)	0.065[a]
Ex-smokers	73.4 (±6.0)		71.8 (±6.4)	
Never-smokers	73.3 (±7.0)		73.2 (±6.4)	
Mean age at start of smoking, years (±s.d.)				
Ever-smokers	19.6 (±3.5)		33.9 (±12.4)	
Current-smokers	19.9 (±4.3)	0.298[b]	36.1 (±13.1)	0.196[b]
Ex-smokers	19.6 (±3.2)		32.7 (±11.9)	
Mean numbers of CPD (±s.d.)				
Ever-smokers	21.1 (±13.0)		13.3 (±8.1)	
Current-smokers	16.6 (±9.1)	<0.001[b]	12.2 (±6.0)	0.604[b]
Ex-smokers	22.7 (±13.7)		13.9 (±9.0)	
Mean numbers of CPD × years (±s.d.)				
Ever-smokers	854 (±582)		402 (±357)	
Current-smokers	852 (±466)	0.057[b]	428 (±304)	0.257[b]
Ex-smokers	855 (±617)		386 (±386)	
Mean FTND score (±s.d.)				
Ever-smokers	3.58 (±2.20)		2.35 (±2.01)	
Current-smokers	3.61 (±2.08)	0.526[b]	2.17 (±1.76)	0.733[b]
Ex-smokers	3.57 (±2.24)		2.47 (±2.17)	
Mean TDS score (±s.d.)				
Ever-smokers	3.07 (±2.48)		2.87 (±2.47)	
Current-smokers	3.75 (±2.41)	<0.001[b]	3.82 (±2.56)	0.022[b]
Ex-smokers	2.84 (±2.47)		2.43 (±2.33)	
Mean number of trial times for quitting smoking in current-smokers (±s.d.)	1.36 (±1.64)		1.24 (±1.55)	
Mean number of trial times for quitting smoking before succeeding in ex-smokers (±s.d.)	2.10 (±1.54)		1.66 (±1.25)	
Drinking status, n (%)[c]				
Current drinkers	853 (52.9)		178 (19.7)	
Ex-drinkers	319 (19.8)		50 (5.5)	
Never-drinkers	442 (27.4)		676 (74.8)	
Lung cancer history, n (%)				
Yes	47 (2.9)		12 (1.3)	
No	1569 (97.1)		893 (98.7)	

Abbreviations: CPD, cigarettes smoked per day; FTND, Fagerström Test for Nicotine Dependence; TDS, Tobacco Dependence Screener.
Ever-smokers: current-smokers and ex-smokers.
[a]Kruskal–Wallis test comparing three statuses.
[b]Mann–Whitney *U* test comparing current-smokers and ex-smokers.
[c]Information about alcohol drinking status were obtained from 1614 male subjects and 904 female subjects.

Table 2 Subjects distribution according to smoking status, lung cancer history and the rs5320 polymorphism of *DBH*

			Smoking status				*Lung cancer history*		
	Genotype	*Total* n *(%)*	*Current-smokers* n *(%)*	*Ex-smokers* n *(%)*	*Never-smokers* n *(%)*	*P-value*[a]	*Yes* n *(%)*	*No* n *(%)*	*P-value*[b]
Males	GG	1275 (78.9)	277 (80.3)	788 (78.5)	210 (78.7)		41 (87.2)	1234 (78.6)	
	AG	319 (19.7)	65 (18.8)	203 (20.2)	51 (19.1)	0.639	5 (10.6)	314 (20.0)	0.195
	AA	22 (1.4)	3 (0.9)	13 (1.3)	6 (2.2)		1 (2.1)	21 (1.3)	
Females	GG	693 (76.6)	22 (73.3)	41 (77.4)	630 (76.6)		7 (58.3)	686 (76.8)	
	AG	200 (22.1)	7 (23.3)	12 (22.6)	181 (22.0)	0.688	5 (41.7)	195 (21.8)	0.277
	AA	12 (1.3)	1 (3.3)	0 (0)	11 (1.3)		0 (0)	12 (1.3)	

[a]The χ^2 tests were performed based on 3×3 tables.
[b]The χ^2 tests were performed based on 3×2 tables.

Table 3 Subjects distribution according to smoking status and lung cancer history

			Smoking status			
	Lung cancer history	*Total* n *(%)*	*Current-smokers* n *(%)*	*Ex-smokers* n *(%)*	*Never-smokers* n *(%)*	*P-value*[a]
Males	Yes	47 (2.9)	2 (0.6)	44 (4.4)	1 (0.4)	<0.001
	No	1569 (97.1)	343 (99.4)	960 (95.6)	266 (99.6)	
Females	Yes	12 (1.3)	0 (0)	1 (1.9)	11 (1.3)	0.689
	No	893 (98.7)	30 (100)	52 (98.1)	811 (98.7)	

[a]The χ^2 tests were performed based on 2×3 tables.

females). Although it may be possible that some kind of population bias exist in this rural population, we tested this genotype if it is in accordance with the Hardy–Weinberg equilibrium. Actually the genotype distribution obeyed the Hardy–Weinberg equilibrium ($\chi^2 = 0.179$, $P = 0.914$ for males and $\chi^2 = 0.332$, $P = 0.842$ for females). Smoking status (current-smokers, ex-smokers and never-smokers) was not significantly different between the three genotypes, nor was lung cancer history.

Table 3 shows subjects distribution according to smoking status and lung cancer history. It shows a significant relationship between lung cancer history and ex-smokers in males ($P < 0.001$); however, there was no significant relationship between the *DBH* rs5320 polymorphism and lung cancer history in male ex-smokers. Most cases of lung cancer history occurred in male ex-smokers with GG genotype, but not statistically significant (Table 4).

The *DBH* rs5320 polymorphism was shown to be of significance in both males and females with regard to FTND, and in males only with regard to CPD (Table 5). Males with AA genotype smoked less cigarettes per day, while those with GG and AG smoked similar number of cigarettes per day. Male ever-smokers with AA genotype also had lower FTND scores than those with AG and GG genotypes, while female ever-smokers with AG genotype had the lowest FTND scores.

Table 4 Subjects distribution according to lung cancer history and the rs5320 polymorphism of *DBH* in male ex-smokers

		Lung cancer history		
Genotype	*Total* n *(%)*	*Yes* n *(%)*	*No* n *(%)*	*P-value*[a]
GG	788 (78.5)	38 (86.4)	750 (78.1)	
AG	203 (20.2)	5 (11.4)	198 (20.6)	0.208
AA	13 (1.3)	1 (2.3)	12 (1.3)	

[a]The χ^2 test was performed based on 3×2 table.

DISCUSSION

The dopaminergic brain pathway is one that has been studied extensively in regards to addictive behaviour due to the shared characteristics of drug abuse to elicit the release dopamine. Because of this, genes involved in dopamine metabolism represent good candidates in the study of addictive behaviours, such as smoking.

This study specifically shows a significant correlation between the CPD in males and FTND in males and females and the *DBH* polymorphism. Males with AA genotype tend to be the least dependent on nicotine, having the lowest CPD and FTND scores, while females with AG genotype had the lowest FTND scores.

DBH polymorphisms have been investigated from the standpoint of DBH deficiency, several neurological diseases, from migraine[18] to attention-deficit hyperactivity disorder,[19] hypertension[20] and cocaine dependence.[21] The promoter polymorphism has been reported to be associated with Alzheimer's disease.[22]

Several polymorphisms of *DBH* have been studied in terms of the association of smoking behaviour. Among them the promoter polymorphism −1021C/T (rs1611115) is the most extensively

Table 5 Comparison of smoking index of ever-smokers according to the rs5320 polymorphism of *DBH*

	Males			*Females*		
Index	n	*Mean ± s.d.*	P-*value*[a]	n	*Mean ± s.d.*	P-*value*[a]
Age at start of smoking						
GG	1062	19.6 ± 3.3		62	33.9 ± 13.2	
AG	268	19.9 ± 4.3	0.593	19	33.9 ± 10.1	0.949
AA	16	20.4 ± 3.0		1	35.0	
CPD						
GG	1065	21.3 ± 13.1		63	13.8 ± 8.4	
AG	268	20.9 ± 12.5	0.007	19	11.2 ± 6.6	0.389
AA	16	13.4 ± 6.1		1	20.0	
CPD × years						
GG	1061	862 ± 598		62	419 ± 377	
AG	268	840 ± 528	0.055	19	334 ± 289	0.557
AA	16	549 ± 226		1	620	
FTND						
GG	983	3.62 ± 2.23		57	2.60 ± 2.02	
AG	251	3.53 ± 2.07	0.044	19	1.53 ± 1.84	0.030
AA	15	2.20 ± 1.42		1	4.00	
TDS						
GG	934	3.08 ± 2.47		51	2.94 ± 2.48	
AG	229	3.10 ± 2.57	0.215	17	2.59 ± 2.58	0.692
AA	15	1.87 ± 1.46		1	4.00	
Times of trial for quitting smoking in current-smokers						
GG	276	1.37 ± 1.68		17	1.38 ± 1.69	
AG	64	1.34 ± 1.48	0.415	7	0.71 ± 1.11	0.557
AA	3	0.33 ± 0.58		1	2.00	
Times of trial for quitting smoking before succeeding in ex-smokers						
GG	698	2.10 ± 1.54		35	1.74 ± 1.28	
AG	182	2.12 ± 1.52	0.916	12	1.42 ± 1.17	0.317
AA	12	2.17 ± 1.59		0	–[b]	

[a]Kruskal–Wallis test.
[b]Not applicable.

investigated as Zabeitian *et al.*[23] reported this polymorphism as a functional polymorphism explaining inter-individual difference of plasma DBH activity. As to its possible association with smoking behaviour, Freier *et al.*[24] reported that individuals who had at least one *DBH*-1021 T allele smoked fewer cigarettes per day than CC homozygotes in relatively small numbers of the European smokers ($n = 220$). Another polymorphism, *DBH* polymorphism T1368A (rs77576840), has been shown to be associated with cigarette consumption.[25]

The tobacco and genetics consortium did a meta-analysis totalling 74 053 subjects and found *DBH* rs3025343 [G] is associated with smoking cessation.[26] Siedlinski *et al.*[27] reported the genome-wide study of chronic obstructive pulmonary disease. They could replicate the result by the above consortium; that is, there was an association between a candidate genotype rs3025343 and smoking cessation in their subjects. The other polymorphisms of *DBH* have been also attempted to correlate with smoking. For example, the rs77905 was investigated in terms of the association with smoking status and nicotine level in 1518 adolescent subjects in United Kingdom, but no association was found.[28] Actually, Breitling *et al.*[29] reported this rs77905 polymorphism did not influence smoking cessation programme including 577 heavy smokers.

The rs5320 polymorphism of *DBH* was investigated as haplotype analysis of Parkinson's disease. Haplotypes rs1611115T > C–rs1108580A > G–rs5320A > G–rs129882C > T are reported to be associated with Parkinson's disease.[13] Our findings that *DBH* rs5320 genotype are associated with smoking behaviour remind us of a well-known observation that Parkinson's disease is less prevalent in smokers and there may be a common genetic root for these status, Parkinson's disease and (addicted) smoking.[30–32] Haplotype block structure of Japanese and Han Chinese population is shown in the Figure 1. Actually, this haplotype block indicates the relatively strong linkage ($r^2 = 0.63$) between rs1108589 and rs5320. Among the single-nucleotide polymorphisms mentioned above, the rs77576840 is not so common and is not listed in the HapMap database. It is between rs302530 and rs1108580. The rs3025343 is outside the figure covers (far 5′ upstream).

As shown previously, numerous polymorphic sites of *DBH* were investigated in various populations. We picked up rs5320 because the prevalence in Japanese is feasible and this is a non-synonymous variation. These polymorphic sites including rs5320 are linked with each other depending on populations. Most of them do not have mechanistic rationale for why these polymorphisms are apparently associated with smoking behaviour, which awaits further investigation. The polymorphism at rs5320, G allele in GCG (Ala) vs A allele in ACG (Thr) at the position 211 of this protein may not have a severe biological effect probably, considering these two amino acids exist alternatively from each other in some of the primates (Figure 2). In regard to our result that males with AA genotype had the lowest CPD and FTND score, the reason why this A allele behaves in a recessive manner is unknown. Effect of amino-acid substitution may influence only when both alleles are variants. An exploration on functional rationale would be warranted.

Interestingly, unlike the FTND scores, no relation was found between the TDS and any of the rs5320 allelotype in our study. This could be due to the fact that the traits detected by the scores of the FTND and TDS are different from each other.[33] Smoking is a personal behaviour that can be attributed to many genetic and environmental factors. The questions in the FTND detect the physical aspects of nicotine dependence, including the one on the value of CPD, whereas those in the TDS tend to focus on the mental aspects of smoking. The TDS is a questionnaire for screening tobacco/nicotine dependence according to some criteria of mental disorder. These characteristics of scales may have led to the result that the CPD and FTND, not TDS in males, were related to the DBH polymorphism significantly. Regarding female subjects, the number of smoker with AA genotype was only one, so the relations between the FTND and this polymorphism should be examined further.

Limitations of this study and its interpretation include the fact that the participants were recruited from a rural city, where demographical and occupational characteristics are different from those living in urban cities or agricultural communities. To validate our observations, replication of this study would need to be done with larger and different populations. This would allow for a larger representation of the various genotypes associated with the *DBH* rs5320 polymorphism and also a larger female sample size, so that one can be able to make a clearer conclusion whether the AA genotype of this locus corresponds

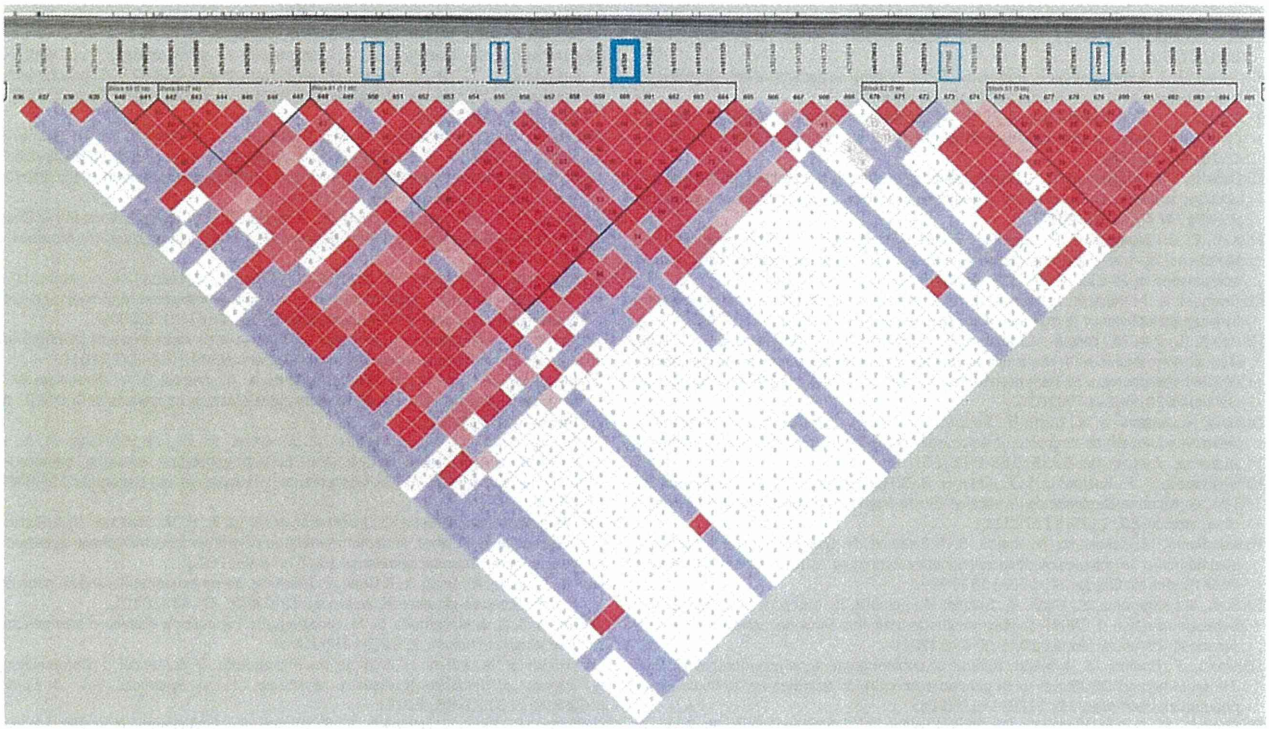

Figure 1 The state of linkage disequilibrium (LD) between the single-nucleotide polymorphisms in the region around the rs5320 polymorphism, which is shown in thick rectangle. The rs1611115, rs77905, rs129882 and rs1108580 are shown in thin rectangles. The strength of LD was calculated based on the genotype data of the Japanese and Han Chinese population extracted from the position 135,474,113 to 135,522,004 on chromosome 9 in the Hapmap database (http://hapmap.ncbi.nlm.nih.gov/index.html.ja).[34] Numbers in squares represent percentage of the r^2 values. Squares without numbers represent $r^2 = 1$. The colour scheme was according to the 'Standard Color Scheme' of the Haploview v.4.1 software (Lod$\geqslant$2, $D' = 1$: bright red; Lod$\geqslant$2, $D' < 1$: shades of pink/red; Lod$<$2, $D' = 1$: blue; Lod$<$2, $D' < 1$: white).[35] The LD blocks were defined based on the default algorithm by Gabriel *et al*.[36]

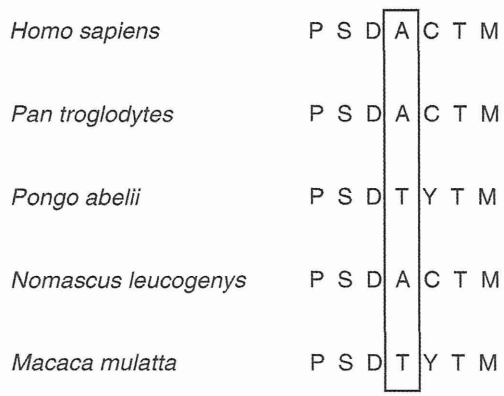

Figure 2 Amino-acid alignment surrounding the position 211 in human and the corresponding positions in the other primates. Though the information on genetic polymorphism in the primates is limited, the database shows this position is Ala or Thr in several primates including human being.

with having a higher FTND score. Recruitment of sample population from a wider demography that is, urban cities and agricultural villages would be needed. This would take into account the different smoking characteristics. Despite these shortcomings, our data has provided a major clue in understanding the smoking behaviour of humans.

CONFLICT OF INTEREST

The authors declare no conflict of interest.

ACKNOWLEDGEMENTS

We acknowledge Dr Kimura at the Hakodate National Hospital for DBH assays. This work was supported by grants-in-aid from the Japanese Ministry of Health, Labour and Welfare for the Comprehensive 10-Year Strategy for Cancer Control and Research on international cooperation in medical science, and from the Japanese Ministry of Education, Culture, Sports, Science and Technology for priority area (221S0001), from the Smoking Research Foundation and from the 21st Century COE programme of the Hamamatsu University School of Medicine.

1 Stewart, L. C. & Klinman, J. P. Dopamine beta-hydroxylase of adrenal chromaffin granules: structure and function. *Annu. Rev. Biochem.* **57**, 551–592 (1988).
2 Weinshilboum, R. M., Thoa, N. B., Johnson, D. G., Kopin, I. J. & Axelrod, J. Proportional release of norepinephrine and dopamine- -hydroxylase from sympathetic nerves. *Science* **174**, 1349–1351 (1971).
3 Smith, A. D., De Potter, W. P., Moerman, E. J. & De Schaepdryver, A. F. Release of dopamine beta-hydroxylase and chromogranin A upon stimulation of the splenic nerve. *Tissue Cell* **2**, 547–568 (1970).
4 Craig, S. P., Buckle, V. J., Lamouroux, A., Mallet, J. & Craig, I. W. Localization of the human dopamine beta hydroxylase (DBH) gene to chromosome 9q34. *Cytogenet. Cell Genet.* **48**, 48–50 (1988).
5 Kobayashi, K., Kurosawa, Y., Fujita, K. & Nagatsu, T. Human dopamine beta-hydroxylase gene: two mRNA types having different 3′-terminal regions are produced through alternative polyadenylation. *Nucleic Acids Res.* **17**, 1089–1102 (1989).
6 Dunnette, J. & Weinshilboum, R. Human serum dopamine beta-hydroxylase: correlation of enzymatic activity with immunoreactive protein in genetically defined samples. *Am. J. Hum. Genet.* **28**, 155–166 (1976).

7 Dunnette, J. & Weinshilboum, R. Inheritance of low immunoreactive human plasma dopamine-beta-hydroxylase. Radioimmunoassay studies. *J. Clin. Invest.* **60,** 1080–1087 (1977).
8 Dunnette, J. & Weinshilboum, R. Family studies of plasma dopamine-beta-hydroxylase thermal stability. *Am. J. Hum. Genet.* **34,** 84–99 (1982).
9 Dunnette, J. H. & Weinshilboum, R. M. Serum dopamine beta-hydroxylase activity in non-human primates: phylogenetic and genetic implications. *Comp. Biochem. Physiol. C.* **75,** 85–91 (1983).
10 Cubells, J. F. & Zabetian, C. P. Human genetics of plasma dopamine beta-hydroxylase activity: applications to research in psychiatry and neurology. *Psychopharmacology (Berl)* **174,** 463–476 (2004).
11 Kim, C. H., Zabetian, C. P., Cubells, J. F., Cho, S., Biaggioni, I., Cohen, B. M. *et al.* Mutations in the dopamine beta-hydroxylase gene are associated with human norepinephrine deficiency. *Am. J. Med. Genet.* **108,** 140–147 (2002).
12 Timmers, H. J., Deinum, J., Wevers, R. A. & Lenders, J. W. Congenital dopamine-beta-hydroxylase deficiency in humans. *Ann. N.Y. Acad. Sci.* **1018,** 520–523 (2004).
13 Punia, S., Das, M., Behari, M., Mishra, B. K., Sahani, A. K., Govindappa, S. T. *et al.* Role of polymorphisms in dopamine synthesis and metabolism genes and association of DBH haplotypes with Parkinson's disease among North Indians. *Pharmacogenet. Genomics* **20,** 435–441 (2010).
14 Sato, N., Kageyama, S., Chen, R., Suzuki, M., Mori, H., Tanioka, F. *et al.* Association between neuropeptide Y receptor 2 polymorphism and the smoking behavior of elderly Japanese. *J. Hum. Genet.* **55,** 755–760 (2010).
15 Heatherton, T. F., Kozlowski, L. T., Frecker, R. C. & Fagerstrom, K. O. The Fagerstrom Test for Nicotine Dependence: a revision of the Fagerstrom Tolerance Questionnaire. *Br. J. Addict.* **86,** 1119–1127 (1991).
16 Kawakami, N., Takatsuka, N., Inaba, S. & Shimizu, H. Development of a screening questionnaire for tobacco/nicotine dependence according to ICD-10, DSM-III-R, and DSM-IV. *Addict. Behav.* **24,** 155–166 (1999).
17 Sato, N., Kageyama, S., Chen, R., Suzuki, M., Tanioka, F., Kamo, T. *et al.* Association between neurexin 1 (NRXN1) polymorphisms and the smoking behavior of elderly Japanese. *Psychiatr. Genet.* **20,** 135–136 (2010).
18 Ghosh, J., Pradhan, S. & Mittal, B. Role of dopaminergic gene polymorphisms (DBH 19 bp Indel and DRD2 Nco I) in genetic susceptibility to migraine in North Indian population. *Pain Med.* **12,** 1109–1111 (2011).
19 Bhaduri, N., Sarkar, K., Sinha, S., Chattopadhyay, A. & Mukhopadhyay, K. Study on DBH genetic polymorphisms and plasma activity in attention deficit hyperactivity disorder patients from Eastern India. *Cell Mol. Neurobiol.* **30,** 265–274 (2009).
20 Chen, Y., Wen, G., Rao, F., Zhang, K., Wang, L., Rodriguez-Flores, J. L. *et al.* Human dopamine beta-hydroxylase (DBH) regulatory polymorphism that influences enzymatic activity, autonomic function, and blood pressure. *J. Hypertens.* **28,** 76–86 (2010).
21 Brousse, G., Vorspan, F., Ksouda, K., Bloch, V., Peoc'h, K., Laplanche, J. L. *et al.* Could the inter-individual variability in cocaine-induced psychotic effects influence the development of cocaine addiction? Towards a new pharmacogenetic approach to addictions. *Med. Hypotheses* **75,** 600–604 (2010).
22 Combarros, O., Warden, D. R., Hammond, N., Cortina-Borja, M., Belbin, O., Lehmann, M. G. *et al.* The dopamine beta-hydroxylase -1021C/T polymorphism is associated with the risk of Alzheimer's disease in the Epistasis Project. *BMC Med. Genet.* **11,** 162 (2010).
23 Zabetian, C. P., Anderson, G. M., Buxbaum, S. G., Elston, R. C., Ichinose, H., Nagatsu, T. *et al.* A quantitative-trait analysis of human plasma-dopamine beta-hydroxylase activity: evidence for a major functional polymorphism at the DBH locus. *Am. J. Hum. Genet.* **68,** 515–522 (2001).
24 Freire, M. T., Marques, F. Z., Hutz, M. H. & Bau, C. H. Polymorphisms in the DBH and DRD2 gene regions and smoking behavior. *Eur. Arch. Psychiatry Clin. Neurosci.* **256,** 93–97 (2006).
25 McKinney, E. F., Walton, R. T., Yudkin, P., Fuller, A., Haldar, N. A., Mant, D. *et al.* Association between polymorphisms in dopamine metabolic enzymes and tobacco consumption in smokers. *Pharmacogenetics* **10,** 483–491 (2000).
26 The Tobacco and Genetics Consortium. Genome-wide meta-analyses identify multiple loci associated with smoking behavior. *Nat. Genet.* **42,** 441–447 (2010).
27 Siedlinski, M., Cho, M. H., Bakke, P., Gulsvik, A., Lomas, D. A., Anderson, W. *et al.* Genome-wide association study of smoking behaviours in patients with COPD. *Thorax* **66,** 894–902 (2011).
28 Huang, S., Cook, D. G., Hinks, L. J., Chen, X. H., Ye, S., Gilg, J. A. *et al.* CYP2A6, MAOA, DBH, DRD4, and 5HT2A genotypes, smoking behaviour and cotinine levels in 1518 UK adolescents. *Pharmacogenet. Genomics* **15,** 839–850 (2005).
29 Breitling, L. P., Twardella, D., Hoffmann, M. M., Witt, S. H., Treutlein, J. & Brenner, H. Prospective association of dopamine-related polymorphisms with smoking cessation in general care. *Pharmacogenomics* **11,** 527–536 (2010).
30 Gu, Z., Feng, X., Dong, X. & Chan, P. Smoking, genes encoding dopamine pathway and risk for Parkinson's disease. *Neurosci. Lett.* **482,** 31–34 (2010).
31 Shahi, G. S. & Moochhala, S. M. Smoking and Parkinson's disease–a new perspective. *Rev. Environ. Health.* **9,** 123–136 (1991).
32 Wirdefeldt, K., Adami, H. O., Cole, P., Trichopoulos, D. & Mandel, J. Epidemiology and etiology of Parkinson's disease: a review of the evidence. *Eur. J. Epidemiol.* **26**(Suppl 1) S1–58 (2011).
33 Sato, N., Sato, T., Nozawa, A. & Sugimura, H. Assessment scales for nicotine addiction. *J. Addict. Res. Ther.* doi:10.4172/2155-6105.S1-008 (2012).
34 International HapMap Consortium. A haplotype map of the human genome. *Nature* **437,** 1299–1320 (2005).
35 Barrett, J. C., Fry, B., Maller, J. & Daly, M. J. Haplotype analysis and visualization of LD and haplotype maps. *Bioinformatics* **21,** 263–265 (2005).
36 Gabriel, S. B., Schaffner, S. F. & Nguyen, H. The structure of haplotype blocks in the human genome. *Science* **296,** 2225–2229 (2002).

Pathology International

Pathology International 2012; **62**: 728–734 doi:10.1111/j.1440-1827.2012.02862.x

Original Article

Chromogenic *in situ* hybridization (CISH) to detect *HER2* gene amplification in breast and gastric cancer: Comparison with immunohistochemistry (IHC) and fluorescence *in situ* hybridization (FISH)

Shinichiro Kiyose,[1,5] Hisaki Igarashi,[1] Kiyoko Nagura,[1] Takaharu Kamo,[1] Kazunori Kawane,[4] Hiroki Mori,[4] Takachika Ozawa,[4] Matsuyoshi Maeda,[6] Keisuke Konno,[5] Hideaki Hoshino,[5] Hiroyuki Konno,[2] Hiroyuki Ogura,[3] Kazuya Shinmura,[1] Naohiko Hattori[5] and Haruhiko Sugimura[1]

Departments of [1]Tumor Pathology, [2]Surgery 2, and [3]Surgery 1, Hamamatsu University School of Medicine, [4]Department of Pathology and Laboratory Medicine, Hamamatsu Medical Center, Hamamatsu, [5]JOKOH, Co., Ltd., Tokyo, and [6]Department of Pathology, Toyohashi Municipal Hospital, Toyohashi, Japan

The chromogenic *in situ* hybridization (CISH) assay, designed to detect the amplification of the *HER2* gene in formalin-fixed, paraffin-embedded (FFPE) breast cancer (BC) and gastric cancer (GC) tissue specimens, was evaluated in 125 FFPE BC cases and 198 FFPE GC cases for which the HER2 status had been predetermined using immunohistochemistry (IHC) and fluorescence *in situ* hybridization (FISH). In the 125 BC cases and the 198 gastric cases, we found a very good concordance (98.4% and 99.0%, respectively) between CISH and FISH. In particular, we evaluated the polysomy cases, as these cases often have ambiguous treatment options in clinical practice. The polysomy of chromosome 17 was defined as the presence of three or more CEP17 signals in at least 10% of the tumor cells. In the 50 BC cases and 54 GC cases displaying chromosome 17 polysomy, the concordance between FISH and CISH was 98.0% and 98.1%, respectively. These results indicate that CISH could provide an accurate and practical alternative to FISH for the clinical diagnosis of *HER2* gene amplification in FFPE BC and FFPE GC samples.

Key words: breast cancer, chromogenic *in situ* hybridization (CISH), fluorescence *in situ* hybridization (FISH), gastric cancer, HER2, immunohistochemistry (IHC)

Correspondence: Haruhiko Sugimura, MD, PhD, Department of Tumor Pathology, Hamamatsu University School of Medicine, 1-20-1 Handayama, Higashi-ward, Hamamatsu, Japan 431-3192. Email: hsugimur@hama-med.ac.jp

Received 14 June 2012. Accepted for publication 13 September 2012.

The human *HER2* oncogene is located on chromosome 17 and encodes a 185-kDa membrane receptor-like protein with tyrosine kinase activity. The *HER2* gene is a member of the human epidermal growth factor receptor gene family.[1,2] Amplification of the *HER2* gene and overexpression of its protein have been demonstrated in 15–25% of breast cancers. This up-regulation is associated with a poor prognosis.[3–5] Trastuzumab (Herceptin) is a monoclonal antibody specific for the HER2 protein. Trastuzumab has been shown to be an effective therapy only in patients whose tumors show *HER2* gene amplification and/or HER2 protein overexpression. Two types of assays can be used for HER2 evaluation: immunohistochemistry (IHC), which detects protein overexpression, and fluorescence *in situ* hybridization (FISH), which assesses gene amplification. The most frequently used method to ascertain the HER2 status in breast cancer specimens is IHC. However, discrepant IHC results are sometimes obtained using formalin-fixed, paraffin-embedded (FFPE) tissues because technical factors, fixation, and the subjective scoring system can affect the quality of the results. Although FISH is a very accurate and sensitive assay for detecting *HER2* amplification, the evaluation of FISH results requires an expensive fluorescence microscope with high-magnification oil immersion objective lenses (x60-100) as well as a digital camera to record the results. FISH can be performed as a dual-color hybridization allowing the simultaneous enumeration of *HER2* and chromosome 17, which supposedly makes it easier to distinguish true *HER2* amplification from an increase in *HER2* copies arising from chromosomal aneusomy. Recently, chromogenic *in situ* hybridization (CISH) has been introduced by several groups

as an alternative to FISH, and assessments of these commercialized products have been reported in previous studies.[6–9] CISH is similar to FISH, except that the *HER2* gene copies are detected using a permanent peroxidase reaction instead of a fluorescent dye. The hybridization results can be viewed using an ordinary transmitted light microscope. Here, we report our experience with CISH using the HISTRA HER2 CISH kit (JOKOH, Tokyo, Japan) for the determination of *HER2* gene amplification in FFPE breast cancer (BC), and gastric cancer (GC) tissue specimens.

MATERIALS AND METHODS

Tumors and tissue microarray

In total, 125 BC and 198 GC were collected from Hamamatsu University Hospital, Hamamatsu Medical Center, and Toyohashi Municipal Hospital. The CISH, FISH, and IHC evaluations were performed in a blinded fashion with the observer unaware of the results of the other assays.

The tissue microarrays were constructed using 3 mm tissue cores according to a previously reported method.[10–12] One core of tumor from the middle portion of a single tissue block was sampled.

IHC

The IHC analyses were performed according to the manufacturer's protocol for the HercepTest™ (DAKO, Glostrup, Denmark). HER2 overexpression was determined as defined in the HercepTest™ kit guide: a score of 0 or 1+ was considered negative, a score of 2+ was considered weakly positive, and a score of 3+ was considered strongly positive.

FISH

The FISH analysis was performed using the PathVysion™ HER-2 DNA probe kit (Abbott Laboratories, Abbott Park, Des Plaines, IL, USA), which includes two directly labeled DNA probes: a locus-specific probe for the *HER2* gene labeled with SpectrumOrange, and an alpha satellite probe that targets the centromere region of chromosome 17 labeled with SpectrumGreen (CEP17). The mean *HER2*/CEP17 ratio was counted in at least 20 tumor cells for each case.

CISH

The CISH analyses were performed according to the protocol provided with the composition reagent in the HISTRA HER2 CISH kit (JOKOH). After deparaffinization, the sections were incubated in the pretreatment solution at 94°C for 20 min, followed by washing with distilled water and digestion with protease solution at 37°C for 5 min. The slides were then washed with distilled water, and ready-to-use digoxigenin-labeled HER2 DNA probe (probe size, 450 kb) was applied to the slides, which were covered with 22 × 22-mm coverslips (10 μL of probe mixture per slide). The sections were denatured on a thermal plate at 94°C for 5 min, and hybridization was performed overnight at 37°C. After hybridization, the slides were washed with SSC at 75°C for 5 min. The endogenous peroxidase activity and unspecific staining were blocked by applying 3% H_2O_2 and blocking reagent, respectively. A mouse anti-digoxigenin antibody was added to the slides hybridized with the HER2 DNA probe for 30 min at room temperature followed by incubation with antimouse-peroxidase polymer for 30 min at room temperature. A 3,3′-diaminobenzidine (DAB) chromogen substrate was used for chromogenic visualization for 10 min at room temperature. The antibody reaction and the peroxidase reaction were performed using automatic dyeing equipment (Autostainer Universal Staining System™, DAKO). The tissue sections were lightly counterstained with hematoxylin and were embedded. The CISH sections were evaluated using a x40 dry objective lens. The non-amplified gene copy number was defined as 1–5 dots per nucleus. Amplification was defined as more than five dots per nucleus or large or small clusters or mixtures of multiple dots and clusters of *HER2* gene per nucleus in >50% of the cancer cells in the tissue area selected for enumeration (we evaluated at least 30 tumor cells for each case).

RESULTS

Performance of CISH

CISH was performed for 125 BC cases and 198 GC cases. Gene copies visualized using CISH were clearly distinguishable using a x40 objective lens in tissue sections counterstained with hematoxylin. Tumors without *HER2* amplification typically showed 1–2 dots per nucleus (when diploid) (Fig. 1a,b) or 3–5 dots in cases of chromosomal aneuploidy. Amplified gene copies typically presented as large intranuclear gene copy clusters (Fig. 1c,d) or as a mixture of multiple dots and clusters (Fig. 1e,f) or as small gene copy clusters. In GC, heterogeneity of the *HER2* gene copy number was observed. Multiple dots (clusters) and a smaller number of dots per nucleus were observed in the same tissue section (Fig. 2).

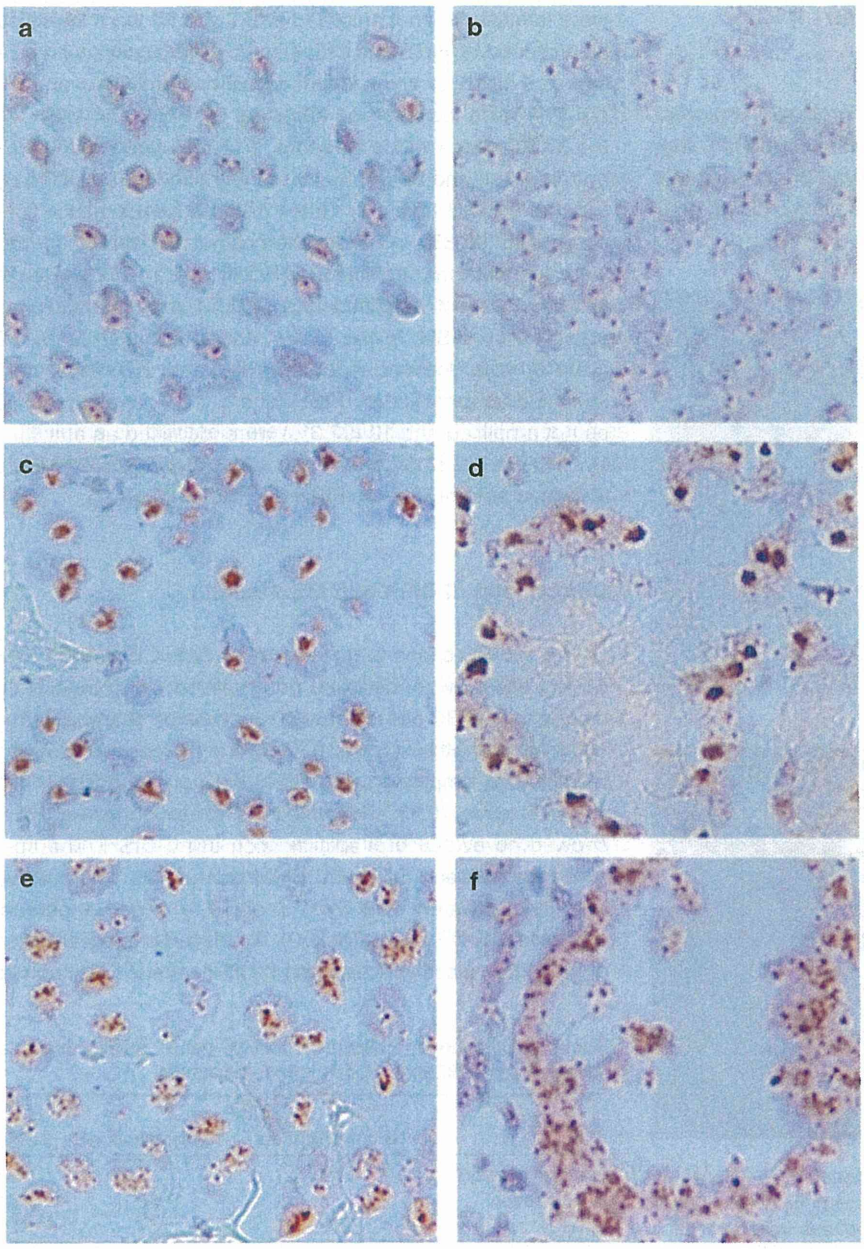

Figure 1 *HER2* chromogenic *in situ* hybridization (CISH) in breast cancers (BC) and gastric cancers (GC). Tumors with no amplification of *HER2* typically showed 1–2 dots per nucleus (BC, **a**; GC, **b**). Amplified gene copies presented typically as large intranuclear gene copy clusters (BC, **c**; GC, **d**) or as a mixture of multiple dots and clusters (BC, **e**; GC, **f**).

Table 1 Correlation between HER2 overexpression as detected using IHC and *HER2* gene amplification as detected using FISH and CISH in breast cancers

	FISH		CISH		
IHC score	No amplification (%)	Amplification (%)	No amplification (%)	Amplification (%)	Total
0	55 (100)	0 (0)	55 (100)	0 (0)	55
1 +	14 (87.5)	2 (12.5)	14 (87.5)	2 (12.5)	16
2 +	4 (23.5)	13 (76.5)	4 (23.5)	13 (76.5)	17
3 +	1 (2.7)	36 (97.3)	1 (2.7)	36 (97.3)	37
Total	74	51	74	51	125

CISH, chromogenic *in situ* hybridization; FISH, fluorescence *in situ* hybridization; IHC, immunohistochemistry.